Available online at www.sciencedirect.com
ScienceDirect
Geochimica et Cosmochimica Acta 70 (2006) 5698–5722
Geochimica
www.elsevier.com/locate/gca

A critical look at iron paleoredox proxies: New insights from modern euxinic marine basins

Timothy W. Lyons *, Silke Severmann

Department of Earth Sciences, University of California-Riverside, Riverside, CA 92521, USA

Received 28 November 2005; accepted in revised form 10 August 2006

Abstract

Enrichments in reactive iron occur under euxinic marine conditions, that is, where dissolved sulfide is present in the water column. These enrichments result primarily from the export of remobilized iron from the oxic shelf, which is scavenged from the euxinic water column during syngenetic pyrite formation and deposited in the underlying sediments. Strongly elevated ratios of highly reactive iron to total iron (Fe_{HR}/Fe_T) and total iron to aluminum (Fe_T/Al) and high degrees of pyritization (DOP) are each products of this enrichment process. These paleoredox proxies are among the most faithful recorders of ancient euxinia.

Contrary to previous arguments, iron enrichment is decoupled from biogenic sediment inputs, but it does appear to be a uniquely euxinic phenomenon. In other words, we can rule out a major contribution from preferential physical transport of Fe_{HR}-rich detrital sediment to the deep basin, which could also operate under oxic conditions. Furthermore, enrichment via the shuttling of iron remobilized from oxic shelves appears to be limited by inefficient transport and trapping processes in deep oxic basins. Elevated Fe_T/Al ratios in the euxinic sediments also cannot be a product of internal enhancement of the reactivity of the detrital iron pool without net Fe_{HR} addition. These conclusions are supported by observations in the modern Black Sea, Orca Basin, and Effingham Inlet.

Fe_T/Al ratios are unambiguous recorders of paleoredox even in sediments that have experienced high degrees of metamorphic alteration. However, this study suggests that high siliciclastic accumulation rates can swamp the enrichment mechanism, resulting in only intermediate DOP values for euxinic sediments and Fe_T/Al ratios that mimic the oxic shelf. Such dilution effects are well expressed in Black Sea basinal turbidites and rapidly accumulating muds on euxinic basin margins. Under conditions of persistent euxinia, varying extents of Fe_{HR} enrichment can illuminate spatial and temporal gradients in siliciclastic sedimentation. The magnitude of enrichment is a function of the source (shelf) to sink (ocean basin) areal ratio, suggesting that iron proxies can also record ocean-scale paleoenvironmental properties through muted enrichments at times of very widespread euxinia. For the first time, manganese data are interpreted in light of the redox shuttle model. As for the iron data, the Black Sea, Orca Basin, and Effingham Inlet show enrichments in total manganese in the deep euxinic basin, suggesting export from the suboxic porewaters of the oxic shelf and scavenging and burial in the basin. The Black Sea data reveal iron and manganese enrichment across the broad, deep euxinic basin, suggesting efficient lateral transport and deep-water mixing tied to the physical properties of the water column.

1. Introduction

Among Bob Berner's groundbreaking contributions to studies of early diagenesis in marine sediments are the lessons he taught us about iron availability as a central player in the coupled cycles of many bioessential elements. Berner (1970) recognized that reactive iron, delivered with detrital sediment, is consumed to varying degrees through reaction with hydrogen sulfide that forms microbially at the expense of labile organic matter. This iron can limit the formation of sedimentary pyrite when abundant supplies of organic carbon and sulfate are available. He also proposed that a 1-min extraction with boiling, concentrated hydrochloric acid can approximate the amount of iron remaining in sediment that is reactive to hydrogen sulfide on early diagenetic time scales. Berner argued that the method efficiently extracts those phases most readily reactive to H_2S (e.g.,

* Corresponding author. Fax: +1 951 827 4324.
E-mail address: timothy.lyons@ucr.edu (T.W. Lyons).

0016-7037/$ - see front matter © 2006 Elsevier Inc. All rights reserved.
doi:10.1016/j.gca.2006.08.021

the iron [oxyhydr]oxides), though only partially extracting the less reactive silicate phases (an observation later corroborated and quantified by Raiswell et al., 1994). Berner (1970) expanded this concept by introducing the *degree of pyritization* (DOP) parameter, defined as pyrite-Fe/(pyrite-Fe + HCl-extractable Fe). From this definition, it followed that sediments with ample remaining supplies of reactive iron have low DOP values, and degrees of pyritization for those with limited iron availability should approach one.

Berner's important work with Rob Raiswell in the 1980s built from the iron relationships he elucidated earlier. Through studies of the modern Black Sea and ancient black shales and their high associated DOP values, and through comparisons to modern and ancient normal marine environments (with oxygen-containing bottom waters), Berner and Raiswell argued that iron-limited pyrite formation is diagnostic of euxinic conditions (Berner and Raiswell, 1983; Berner, 1984; Raiswell and Berner, 1985, 1986; Lyons and Berner, 1992; also Leventhal, 1983). Euxinic settings are defined as having anoxic *and* hydrogen sulfide-containing bottom waters. By corollary, Berner and Raiswell suggested that organic matter is generally limiting in normal marine settings, and sulfate is limiting under freshwater to brackish conditions. In euxinic water columns, bacterial sulfide production occurs ubiquitously; local sedimentary pyrite concentrations and organic carbon delivery are therefore decoupled. Conversely, in normal marine settings, sulfide production is restricted to anaerobic porewaters and thus is intimately coupled to and controlled by *local* availability of organic matter. Berner and Raiswell asserted that more pyrite forms in euxinic environments with higher degrees of pyritization because of the long exposure to high levels of H_2S, resulting in sulfidation of the less reactive iron minerals—that is, those phases only weakly soluble in boiling, concentrated HCl. This condition would be enhanced under the comparatively sediment-starved circumstances of most euxinic, deep basinal environments. From these observations, Raiswell et al. (1988) delineated a still widely embraced scheme for estimating paleoredox, which they calibrated using ancient shales with independent paleoecological indications of oxic to weakly oxic to anoxic/sulfidic bottom waters. According to Raiswell et al., these facies show low (<0.42), intermediate ($0.46 < \text{DOP} < 0.80$), and high ($0.55 < \text{DOP} < 0.93$) degrees of pyritization, respectively, with the potential for some overlap.

More than two decades later, the idea of iron limitation under euxinic conditions remains a central theme in biogeochemical studies. Thanks to continued work by Berner's colleagues and students (in particular Rob Raiswell and Don Canfield), we now have an even firmer grasp of the mechanism behind the DOP paleoproxy. Rather than eroding the utility of the approach, this refinement has enhanced its strength and has facilitated a resurgence of its use within the geological community. In fact, DOP and related Fe_{HR}/Fe_T and Fe_T/Al ratios are now our most dependable inorganic geochemical recorders of ancient local euxinia in fine-grained siliciclastic sediments. When coupled to other approaches, such as molybdenum isotope measurements (Arnold et al., 2004) and concentration relationships (Algeo, 2004; Algeo and Lyons, 2006), the extents of anoxia may be evaluated on a global scale. This paper, through discussions of past work and the inclusion of new results from three modern anoxic basins, explores how and where Fe-based paleoredox proxies work and what more we can hope to learn about ancient environments directly or indirectly from iron geochemistry and its relationship to sedimentary pyrite formation.

This exploration is meant to expand the paleoenvironmental utility of iron geochemistry by emphasizing, for example, the total iron data that are common in past black shale and paleoceanographic literature and stressing the full range of geologic processes that control iron distributions in sediments, including siliciclastic accumulation rates. This paper will look forward in light of new iron isotope methods and heightened interest in constraining paleoredox. Studies are now finding increasingly strong links between ancient euxinia and the evolution (e.g., Anbar and Knoll, 2002) and extinction (e.g., Grice et al., 2005; Kump et al., 2005) of eukaryotic organisms. But it is difficult to imagine any of this success without the paths first defined and still illuminated by the research of Bob Berner.

2. Background

High DOP values are consistently indicative of modern and ancient euxinic sediments, and low values reflect oxic deposition. Yet despite DOP's long-recognized, empirically grounded utility, the mechanistic theory behind the iron proxy and specifically the high DOP values of euxinic sediments remained poorly known. More recent work has explored this relationship through very specific arguments about how reactive iron is distributed and transported within euxinic basins, which is clarifying why high DOP values almost invariably record euxinia yet such settings can also show a range of values from high to intermediate.

2.1. Redefining reactive iron

Sedimentary iron research advanced significantly with the publication of Canfield et al. (1992). Canfield and colleagues demonstrated at the FOAM site in Long Island Sound that DOP is intermediate (~0.4) despite exposure to porewater sulfide concentrations of up to 6 mM on time scales of 10^3 years. This observation is in contrast to the modern Black Sea where most of the pyrite forms rapidly in the euxinic water column and results in high DOP values approaching 0.8 (Calvert and Karlin, 1991; Muramoto et al., 1991; Lyons and Berner, 1992; Calvert et al., 1996; Lyons, 1997; Wilkin et al., 1997; Wilkin and Arthur, 2001; Lyons and Berner, 1992). The unavoidable conclusion advanced by Canfield et al. is that the boiling, concentrated (12 N) HCl extraction overestimates the pool of reactive

iron, because in addition to amorphous and crystalline Fe-oxides that are readily reactive to H_2S on early diagenetic time scales, it also dissolves a significant proportion of silicate-bound Fe that is not reactive to H_2S. By inference, the high DOP values that typify euxinic sediments must stem from controls other than duration of exposure to high concentrations of dissolved sulfide. At the same time, extraction schemes calibrated carefully to pure mineral phases and well-constrained natural sediments were redefining the composition of the sedimentary iron pool and the relative time scales of reactivity to H_2S for the various iron-bearing minerals present (Canfield, 1989; Canfield et al., 1992; Raiswell et al., 1994). From this work, much of the emphasis shifted subtly away from DOP toward exploration of other iron proxies that quantify the most highly reactive iron present within a variety of sedimentary systems.

The most highly reactive iron phases in sediments, dominantly oxides and oxyhydroxides, are reactive toward H_2S on time scales of only days to weeks or less (Canfield et al., 1992; Poulton et al., 2004a). With this framework, Canfield et al. (1996) investigated the relationship between iron present in sulfide minerals and the total iron content of sediments in the Black Sea and found that the classic Unit 1 microlaminated deposits of the deep basin were enriched in sulfide-associated reactive iron by a factor of 2–3 compared to highly reactive iron concentrations in sediments from a variety of normal marine settings. Canfield et al. attributed these enrichments in reactive iron to the scavenging of dissolved iron in the water column during (syngenetic) pyrite formation within settling, organic-rich particulates characterized by rapid local rates of bacterial sulfate reduction. By contrast, all the pyrite associated with oxic to suboxic bottom waters forms (diagenetically) within the sediments, and such iron enrichment cannot occur.

The next challenge was a precise definition and quantification of reactive iron, particularly given that in many types of sediment only a portion of the total reactive iron pool is converted to iron sulfide. Canfield (1989) explored the distributions of reactive iron in marine sediments through a series of chemical extractions. Building from past work (e.g., Mehra and Jackson, 1960), Canfield used a buffered (pH 4.8) citrate–dithionite solution to extract all the iron from the major iron (oxyhydr)oxide minerals (ferrihydrite, lepidocrocite, goethite, and hematite), with only minor contributions from silicate minerals (a specificity later quantified by Raiswell et al., 1994). Based on studies of natural systems (e.g., Canfield, 1989; Canfield et al., 1992), this fraction was shown to be a better measure of iron that is rapidly reactive toward H_2S. From this observation, the pool of highly reactive iron (Fe_{HR}) can be defined as the sum of (1) pyrite-Fe; (2) iron present as acid-volatile sulfide (AVS), comprising the suite of pyrite precursor phases with a stoichiometry closer to iron monosulfide (“FeS”); and (3) residual, unsulfidized dithionite-extractable Fe (Raiswell and Canfield, 1996, 1998). Consistent with the concern that the standard DOP method may overestimate the pool of readily reactive iron, Raiswell and Canfield (1996) demonstrated that boiling, 12 N HCl extracts poorly reactive iron (Fe_{PR}) from silicate minerals that are sulfidized only on a 10^6-year time scale (in the extreme, commonly 10^4–10^5 years; Canfield et al., 1992). Total iron (Fe_T) can thus be thought of as the sum of (1) Fe_{HR}, (2) Fe_{PR}, and (3) iron that is essentially unreactive to H_2S and is insoluble in boiling HCl (Fe_{UNR} occurring dominantly in silicate phases). Poulton and Canfield (2005) recently refined the analytical characterization of reactive iron to permit determinations of Fe(II)-containing but unsulfidized iron minerals (magnetite and iron carbonates), which become particularly important in distinguishing between iron-limited and sulfur-limited conditions in, for example, the Precambrian ocean.

2.2. Iron recycling, enrichment, and the shelf-to-basin iron shuttle

Recent studies of iron speciation in sediments from euxinic and normal marine basins have confirmed the observations first made by Canfield et al. (1996) that Fe_{HR} enrichments are diagnostic of deposition beneath a sulfidic water column (Raiswell and Canfield, 1996; Wijsman et al., 2001; Lyons et al., 2003). The mechanism now commonly proposed for this enrichment is intrabasinal mobilization of iron from the shallow shelf to the deep basin, where it is fixed and deposited through syngenetic pyrite formation in the euxinic water column (Canfield et al., 1996; Lyons, 1997; Wijsman et al., 2001; Lyons et al., 2003; Raiswell and Anderson, 2005), although enhanced reactivity of the detrital iron pool has also been suggested (Anderson and Raiswell, 2004). The implication is that the syngenetic iron augmentation is decoupled from the *local* flux of siliciclastic sediment and thus the aluminum content of the sediment (Fig. 1; Canfield et al., 1996). Evidence for syndepositional reactive iron enrichment is based on the observation that ratios of Fe_{HR} to Fe_T are typically elevated in euxinic basin sediments (e.g., ~0.6 to 0.7 for uppermost Holocene Unit 1 sediments of the Black Sea; Raiswell and Canfield, 1998; Anderson and Raiswell, 2004) relative to the global weighted average for modern riverine particulates (0.43 ± 0.03; Poulton and Raiswell, 2002). Fe_{HR}/Fe_T ratios for the riverine sediments are, in turn, high compared to globally distributed, oxically to suboxically deposited continental margin and deep sea sediments (0.26 ± 0.09; Raiswell and Canfield, 1998; Anderson and Raiswell, 2004).

Through the hypothesized intrabasinal shuttle, reactive iron is repartitioned from the oxic/subxoic shelf to the iron sulfide pool of the euxinic deep basin (Raiswell and Canfield, 1998; Wijsman et al., 2001; Anderson and Raiswell, 2004). Export of reactive iron from shelf sediments results from solubilization of iron (oxyhydr)oxides during diagenesis and release of dissolved Fe(II) into the water column (Fig. 2). For sediments above the chemocline, a large proportion of this $Fe(II)_{aq}$ flux is expected to reoxidize at the sediment–water interface and redeposit with the shelf sediments as iron oxyhydroxide, where it can be recycled many

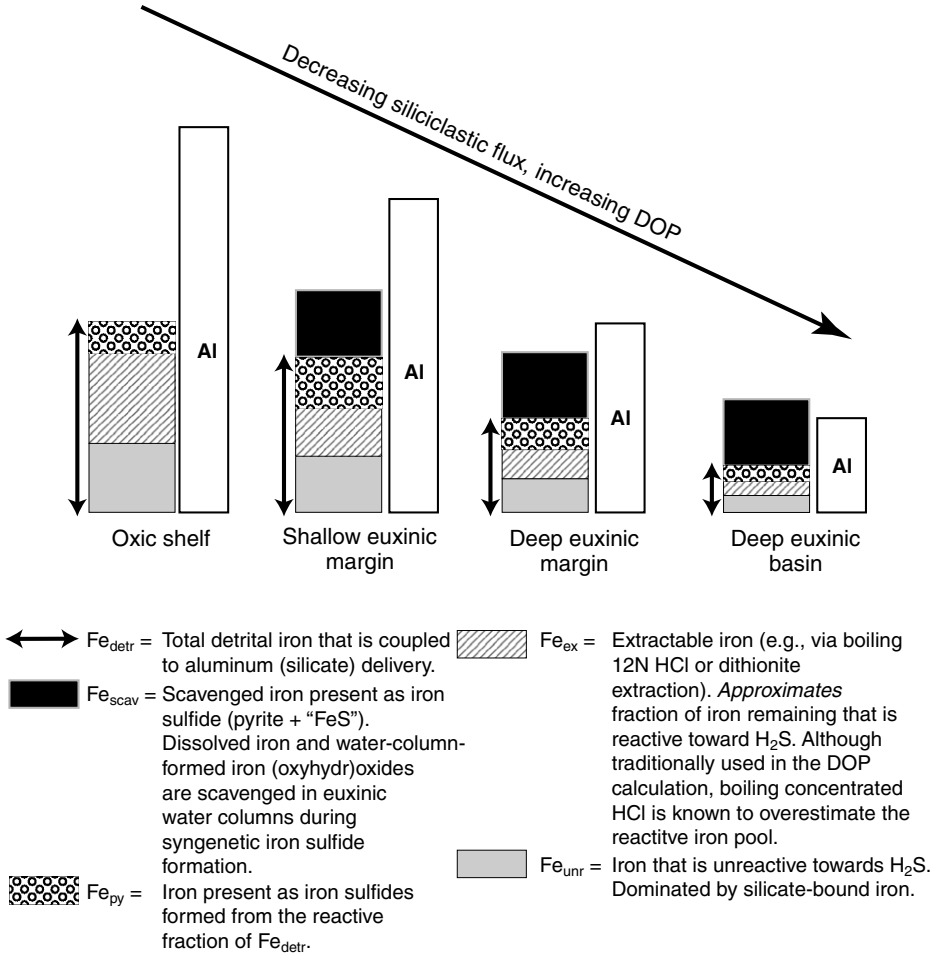

Fig. 1. Summary of iron speciation in fine-grained siliciclastic sediments and sedimentary rocks as it might be found in a transect from the oxic shelf to the deep euxinic basin. The detrital (=siliciclastic) flux is assumed to decrease with increasing distance from land, whereas the euxinic Fe augmentation (Fe_{scav}) is kept constant below the chemocline in this example. Further, we ignore the effects of carbonate dilution, which would affect the total concentrations but not the elemental ratios. Irrespective of carbonate dilution or changes in the siliciclastic flux, the Fe_{detr}/Al ratio remains constant, and any increase in Fe_T/Al indicates euxinic iron enrichment. Only a fraction of Fe_{ex} is pyritized during prolonged exposure to H_2S anoxia in the sediments, whereas augmented Fe_{scav} is quantitatively pyritized during syngenetic pyrite formation in the water column. In the modern Black Sea, the siliciclastic flux along the shallow euxinic margin is actually greater than that of the oxic shelf, thus swamping Fe_{scav}.

times. However, a significant fraction of the benthic $Fe(II)_{aq}$ flux appears to escape redeposition to the sediments and is transferred to the deep basin (Raiswell and Canfield, 1998; Wijsman et al., 2001; Anderson and Raiswell, 2004). Shelf-to-basin reactive iron transport may occur through advection of either dissolved iron or fine-grained particulate iron oxyhydroxides, but the relative importance of these two mechanisms remains speculative (Anderson and Raiswell, 2004).

In the sulfidic water column, the iron transported laterally from the shelf is efficiently sequestered by iron-sulfide precipitation under iron-limited conditions and thus added to the reactive pool of the basinal sediments (Wijsman et al., 2001; Anderson and Raiswell, 2004). Euxinic iron enrichments are therefore a function of the escape efficiency of iron from benthic shelf-recycling, as well as the relative proportions of shelf area to basin area—that is, the source-to-sink ratio (Raiswell and Anderson, 2005). The escape efficiency for sediments is poorly constrained but is probably controlled by the depth of oxygen penetration, porewater Fe(II) concentration, porewater pH, and bottom-water oxygen availability (Raiswell and Anderson, 2005). In addition, the net escape efficiency from a continental shelf must take into account repeated cycles of benthic release (reduction) and redeposition (oxidation) of reactive iron during its lateral advection across the shelf. Reactive iron delivery by riverine particulates to oxic/suboxic shelf regions, followed by selective remobilization, transport, and deposition in the deep euxinic basin, is consistent with the Fe_{HR}/Fe_T relationships outlined above for the three sediment reservoirs—specifically, the respective deficiencies and enrichments for the coastal and deep euxinic sediments compared to the river-transported, continental source. Despite the importance of this general relationship,

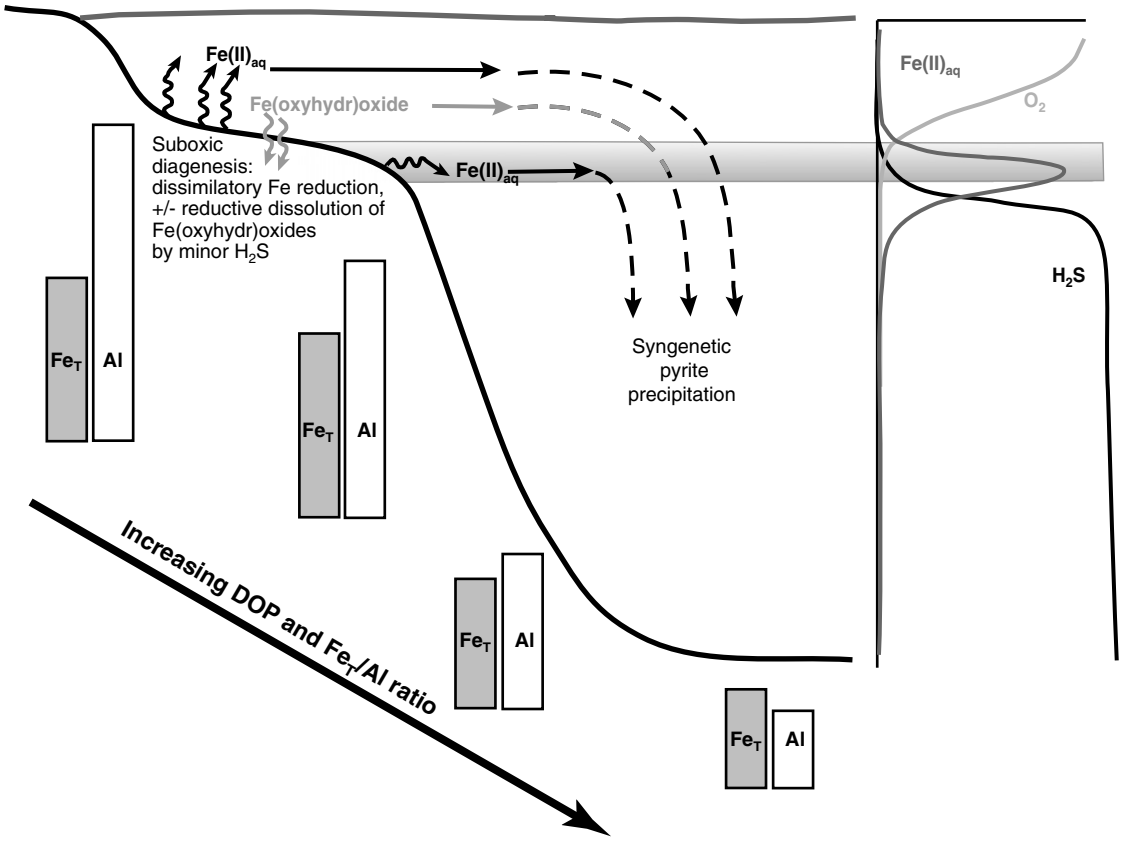

Fig. 2. Schematic diagram illustrating the shuttling mechanism of reactive iron from the oxic shelf to the euxinic basin (after Raiswell and Anderson, 2005). Stacked Fe and Al figures (simplified from Fig. 1) show the effect of decreasing siliciclastic flux and increased reactive Fe enrichment on the Fe_T/Al ratio. Sediments on the shelf, containing lithogenous iron sources, undergo suboxic diagenesis and generate dissolved Fe(II) that diffuses into the overlying bottom waters. Most of the iron is likely to be reoxidized at the sediment–water interface and recycled to the sediments as iron oxyhydroxide. However, a significant proportion is transported to the deep basin, where it is sequestered in the euxinic water column as iron-sulfide. The speciation of the iron during transport is not clear but is likely to be ligand-bound dissolved iron or fine-grained particulate iron oxyhydroxide. In the chemocline, $Fe(II)_{aq}$ is exported without oxidative recycling to the sediments; however, due to the small areal extent of the chemocline/shelf interface, this mechanism can only account for a small proportion of the total shelf-basin iron flux.

comparisons to riverine particulates are complicated by loss of iron oxides in estuaries, prior to transport and deposition on the shelf (Dai and Martin, 1995; Wen et al., 1999). In the discussion below we will deemphasize riverine data in favor of comparisons between oxic/suboxic and euxinic sediments within a given basin—thus highlighting the source–sink relationship—and relative to other marine sediments and average shale. This choice is further justified by the absence of riverine data for the basins we studied.

A more effective mechanism for shelf-to-basin transport is extraction of reactive iron from the zone where the chemocline intersects the seafloor (Fig. 2). Within the chemocline, $Fe(II)_{aq}$ may be transported laterally with minimal oxidative recycling and redeposition on the shelf. Chemocline extraction, however, is limited by the relatively small area of its intersection with the seafloor. Vertical fluctuations in the position of the chemocline (Lyons et al., 1993; Sinninghe Damsté et al., 1993) would amplify this process only moderately. It is also possible that the reactivity of particulate iron in the deep basin is enhanced by mechanisms that are not well understood (Anderson and Raiswell, 2004) but potentially involve microbial activity (Kostka et al., 1999; Li et al., 2004) or grazing by heterotrophic organism (Barbeau and Moffett, 2000) as particles settle through the sulfidic water.

Anomalously high *oxic* DOP values that are apparently restricted to coastal lagoons and salt marshes are exceptions to the rule (Roychoudhury et al., 2003; Neumann et al., 2005). In these settings, intense physical and biological reworking and associated short-term vacillations in sediment redox can act to recycle, remobilize, and locally concentrate labile iron within the sediments (Aller et al., 1986; Canfield, 1989; Rude and Aller, 1989; Aller et al., 2004), and coastal settings can focus the deposition of riverine sediments with unusually high reactive iron reservoirs. These exceptions point to the importance of viewing iron proxies within a broad sedimentological, paleoecological, and sequence stratigraphic context, which should point independently to transitional, nearshore conditions of deposition. Phanerozoic examples of such settings should also show clear, independent paleoecological evidence for oxic deposition.

Regardless of the specific reaction (biotic versus abiotic, etc.) and transport pathways involved, pronounced Fe_{HR} enrichments typify most euxinic sediments (Raiswell and Canfield, 1998), and it is these enrichments, rather than prolonged exposure to high concentrations of H_2S, that explain the high DOP values also observed in these settings. The shelf-source (shuttle) model was first developed and quantitatively validated through measurements and numerical modeling of dissolved iron fluxes out of sediments on the Black Sea shelf (Wijsman et al., 2001) and more recently through a model that thoroughly tracks the iron mass balance in the Black Sea (Anderson and Raiswell, 2004). Both studies suggest that measured and modeled fluxes of iron from the margin are adequate to account for the Fe_{HR} enrichments observed in the deep basin. A recent model has extended the general relevance of the shuttle mechanism to include all modern and ancient euxinic settings (Raiswell and Anderson, 2005). Like DOP, Fe_{HR}/Fe_T ratios have proven their value in the recognition of ancient euxinia (Raiswell et al., 2001; Shen et al., 2003; Poulton et al., 2004b). Unlike DOP, however, these ratios are linked uniquely to sedimentary distributions of the most highly reactive phases of iron, which elevates their sensitivity to the environmental parameters that modulate Fe_{HR} enrichment—with paleoredox as the central factor.

3. Materials and methods

3.1. Sample descriptions

Previously unpublished data are presented from a range of oxic, suboxic, and euxinic settings in the Black Sea, Orca Basin, and Effingham Inlet. With the exception of total iron and aluminum concentrations, which are not vulnerable to storage artifacts, all geochemical analyses were performed soon after collection. The Black Sea is the largest permanently anoxic basin in the modern ocean, with anoxic and sulfidic waters below ~100 m and extending to the seafloor at depths in excess of 2000 m in the central basin. The Black Sea locations, cores, and samples used in this study are described in exhaustive detail elsewhere, including a broad range of complementary geochemical results (Lyons, 1991, 1992, 1997; Lyons and Berner, 1992; Lyons et al., 1993; Anderson et al., 1994; Canfield et al., 1996; Hurtgen et al., 1999; Lyons and Kashgarian, 2005). Rather than recapping the full breadth of previous results, a summary is provided here and in Table 1. Other details are presented in Section 5. Briefly, box cores from Stations 9 and 14 of the 1988 R/V *Knorr* Black Sea cruise were collected in the deep (>2000 m), central euxinic basin and consist entirely of microlaminated, coccolith-rich *Unit 1* mud (using the nomenclature of Ross et al., 1970; also Ross and Degens, 1974; Hay et al., 1991; Arthur et al., 1994; Arthur and Dean, 1998). The upper ~17 cm at Station 18A, also in the deep euxinic center, is a compositionally and texturally homogeneous muddy turbidite conformably underlain by Unit 1 sediment. Organic carbon and calcium carbonate concentrations in Unit 1 sediment at Stations 9, 14, and 18A average 5.3 ± 1.0 and 52.5 ± 11.3 ($\pm 1\sigma$) wt%, respectively.

Table 1
Summary of locations, water depth and sediment characteristics for cores discussed in this study

Location	Depositional environment	Core #s	Water depth (m)	General sediment properties
Black Sea	Oxic shelf	3	85	Gray to brown mud; highly bioturbated with thin oxidized surface layer; discrete burrow traces visible; shell-rich.
		4	115	
		16	129	
		17	97	
Black Sea	Chemocline	16B	160	Grayish brown mud with dark-gray to black bands; transitional character with discrete burrows; minor shelly fauna; disturbed lamination.
Black Sea	Shallow euxinic margin	5	233	Rapid accumulation rates; water-rich; mm-to cm-scale color banding of alternating dark gray and jet black sediment.
		15	198	
Black Sea	Deep euxinic margin	7	1949	Muddy gray turbidites with strong textural homogeneity; well-developed surface fluff layer; erosion-free basal contact at depth.
Black Sea	Euxinic basin	9	2094	Microlaminated sediments (Unit 1) with surface flocculent layer; mm-scale banding: white layers rich in coccolithophores and dark-gray layers predominantly siliciclastic; surface of Station 18A turbiditic (see Station 7).
		14	2218	
		18A	2150	
Orca Basin	Oxic basin margin	LH996 KC8	2039	Surface 6 cm consists of olive-brown, water-rich, bioturbated mud; underlain by light-gray, bioturbated, cohesive mud.
Orca Basin	Chemocline	LH996 BC7	2240	Dramatic brick-red color mottled with light-gray mud; subtle cm-scale banding.
Orca Basin	Euxinic basin	LH996 BC6	2336	Black microlaminated (mm-to cm-scale) mud; water-rich; containing well-preserved Sargassum and carbonate and siliceous microfossils.
Effingham Inlet	Oxic outer basin	EF2-GC7	121	Gray-brown muds with black mottles near surface; strongly bioturbation with open burrows at sediment–water interface; abundant shell fragments; presence of terrestrial organic matter (pine needles, twigs).
Effingham Inlet	Euxinic inner basin	EF1-GC3	120	Black microlaminated (mm-scale) mud; gravtiy flow below 30 cm depth.

The data reported here from Station 7 in the deep but marginal euxinic basin are from two stacked, similarly homogeneous, gray muddy turbidites with average organic carbon and calcium carbonate contents of 1.3 ± 0.1, 10.9 ± 1.1 wt%, respectively. These values are slightly lower than the organic carbon and calcium carbonate concentrations in the turbidite layer from Station 18A, which average 2.0 ± 0.3 and 15.6 ± 1.7 wt%, respectively. Data from background, hemipelagic material between and overlying the turbidites were excluded from these mean values. Sediments from Stations 5 and 15 were collected along the basin margin on the upper slope in euxinic waters immediately below the chemocline at depths of ~200 m. These soupy muds are characterized by alternating, millimeter- to centimeter-scale dark gray and black color bands reflecting high concentrations of AVS. This color banding is superimposed on a finer-scale, undisturbed lamination revealed in X-radiographs. Below the surface interval characterized by progressive remineralization of organic matter, organic carbon and calcium carbonate concentrations average 1.7 ± 0.4 and 12.4 ± 1.3 wt%, respectively, at the two stations. Station 16B was positioned within the low oxygen transition that marks the impingement of the chemocline with the seafloor on the basin margin. Predictably, the sediments here show a transitional fabric, with evidence for less distinct lamination—compared to Unit 1—and bioturbation that becomes more pronounced below about 22 cm. Prominent millimeter-scale black bands in the upper 22 cm mark AVS enrichment. Organic carbon and calcium carbonate contents at 16B average 0.9 ± 0.1 and 18.1 ± 1.8 wt%, respectively. Stations 3, 4, 16, and 17 were on the shallow oxic shelf, with sediments characterized by varying amounts of shelly material and high degrees of bioturbation. Below the surface interval, organic carbon and calcium carbonate concentrations at the four stations collectively average 1.3 ± 0.4 and 20.1 ± 5.3 wt%, respectively. At these sediment depths, organic carbon concentrations are roughly asymptotic. Sediments from Stations 5, 15, and 16B were the only samples with levels of AVS-S appreciably above the detection limits of approximately 10^{-2} wt%.

Sedimentation rates determined from varve counts and radiocarbon and ^{210}Pb analyses are available from these and similar sites within the Black Sea. Estimates from the different methods have converged on roughly 15–20 cm/kyr for Unit 1 in the deep basin (Calvert et al., 1991; Crusius and Anderson, 1992; Arthur et al., 1994; Jones and Gagnon, 1994; Arthur and Dean, 1998). Conversely, ^{210}Pb data (corroborated by Cs trends) yield sedimentation rates of 670 and 770 cm/kyr for Stations 5 and 15, respectively (Moore and O'Neil, 1991; Anderson et al., 1994; Lyons and Kashgarian, 2005; R. Anderson, unpublished data; data are unavailable for Station 4). Rates at Stations 3, 16, 17, and 16B are approximately 60, 60, 90, and 110 cm/kyr (Anderson et al., 1994; R. Anderson, unpublished data; data are unavailable for Station 4). Accumulation of the muddy turbidites (Stations 7 and 18A) can be thought of as essentially instantaneous, with surprising little erosion of the underlying sediment (Crusius and Anderson, 1991).

The Orca Basin is an intraslope, 400 km^2 depression in the northern Gulf of Mexico with a depth range of about 1800–2400 m. The deepest ~200 m of the depression are filled with a brine with a salinity nearly 10 times that of normal seawater (Shokes et al., 1977; Sheu, 1990). This brine pool is stably stratified and permanently anoxic (Sheu, 1990; Van Cappellen et al., 1998). Sediments were cored at three sites—LH996 BC6, LH996 BC7, and LH996 KC8—characterized by euxinic, oxic, and transitional deposition, respectively. The transitional site is within the chemocline, whose redox geochemistry has been well studied by Van Cappellen et al. (1998). Sample methods, locations, and sediment properties are thoroughly described in Hurtgen et al. (1999), along with a broad suite of geochemical data that complement the results and goals of this study. Briefly (also Table 1), sediments from LH996 BC6 consist entirely of soupy, black (AVS-rich) microlaminated mud with well-preserved carbonate and siliceous planktonic microfossils throughout. Organic carbon and calcium carbonate contents average 2.2 ± 0.9 and 20.0 ± 5.3 wt%, respectively. The upper 43.5 cm of sediment from the transitional (chemocline) site, LH996 BC7, are strikingly brick red with suggestions of light gray mottling. X-radiographs reveal a subtle centimeter-scale banding within this red interval. Below the red zone (to the base of the core at 52 cm) the mud is dominantly light gray. Organic carbon and calcium carbonate contents average 0.5 ± 0.1 and 12.1 ± 3.0 wt%, respectively. The sediments from the oxic site (LH996 KC8) consist of homogeneous, bioturbated olive-brown (upper 6 cm) to light gray mud with average organic carbon and calcium carbonate contents of 0.7 ± 0.1 and 19.7 ± 0.8 wt%, respectively. Sedimentation rates in excess of 60 cm/kyr have been reported for the euxinic muds (Addy and Behrens, 1980; Leventer et al., 1983).

Sample methods, locations, and sediment properties for Effingham Inlet are detailed in Hurtgen et al. (1999), Ingall et al. (2005), and Table 1. Effingham Inlet is a fjord on the southwestern coast of Vancouver Island that extends for 17 km with a width of about 1 km. There are two sills within the basin—at outer and inner locations—with water depths of 70 and 40 m, respectively. The outer basin reaches a water depth of ~210 m, and the inner basin is about 120 m at its deepest point. No major rivers enter the inlet. Euxinic site EF1 GC3 (at 120 m depth) is in the inner basin; the oxic–anoxic interface is at a depth of ~60 m. EF2 GC7 in the outer basin (also with a depth ~120 m depth) has weakly oxic bottom waters that are just above the sub-basin's oxic–anoxic interface. Despite the low oxygen content, sediments in the EF2 GC7 core are homogeneous, bioturbated, gray-brown muds with open burrows at the sediment–water interface and small shell fragments throughout. Black (AVS) mottles were observed in the upper few centimeters, and terrestrial plant debris is abundant with average organic carbon and calcium carbonate contents of 0.6 ± 0.1 and 4.0 ± 1.3 wt%, respectively. Mud cored at EF1 GC3 is black (AVS-rich) and microlaminated (Table 1). Organic carbon and calcium carbonate contents in the euxinic sediments average 0.5 ± 0.2 and 4.0 ± 1.3 wt%, respectively. Sedimentation rates based on ^{210}Pb distributions are 300 cm/kyr at EF1 GC3 and 700 cm/kyr at EF2 GC7 (Ingall et al., 2005). Rates of 500 cm/kyr for both cores determined from subsurface ^{137}Cs maxima are in general agreement with the ^{210}Pb results.

3.2. Analytical methods

Total iron (Fe_T), manganese (Mn_T), and aluminum (Al) were extracted from bulk, dried powders using $HF/HHO_3/HClO_4$ digestions and quantified via inductively coupled plasma–atomic emission spectrometry (ICP-AES). Replicate Fe_T, Mn_T, and Al analyses generally agree within a few percent. Splits of bulk powders were also analyzed for concentrations of total reduced inorganic sulfur (TRIS: pyrite-S + AVS-S + elemental-S) using the chromium reduction method (Canfield et al., 1986). For many samples—including all those with appreciable AVS concentrations—wet, homogenized, freshly thawed samples were extracted for concentrations of AVS-S using 6 N HCl with 15% $SnCl_2$ at room temperature (Chanton and Martens, 1985). Pyrite-S concentrations were then determined by chromium reduction of the HCl-insoluble residue. We did not perform separate extractions for elemental sulfur, but we assume these concentrations are relatively small compared to those for AVS-S and pyrite-S. Sulfur recoveries of 96–98% for chromium reduction are typical for freshly ground pyrite standards, and marine samples generally show ±2% or better reproducibility. Our recoveries for CdS standards using the HCl–$SnCl_2$ method averaged 98%. Our past work has confirmed that sulfur in AVS oxidizes during drying and storage to a phase (likely S°) that is still extractable during chromium reduction.

Concentrations of AVS-Fe and pyrite-Fe were calculated assuming "FeS" and "FeS_2" stoichiometries, respectively. From these data, we calculated DOP and DOS (for samples with appreciable AVS):

$$\mathrm{DOP} = \frac{\text{pyrite-Fe}}{\text{pyrite-Fe} + \text{extractable-Fe}} \quad \text{and}$$

$$\mathrm{DOS} = \frac{\text{pyrite-Fe} + \text{AVS-Fe}}{\text{pyrite-Fe} + \text{AVS-Fe} + \text{extractable-Fe}},$$

where "extractable-Fe" is operationally defined (as outlined above) as iron dissolved after 1 min in boiling, 12 N HCl (Berner, 1970; Raiswell et al., 1988). Boesen and Postma (1988) defined degree of sulfidization, DOS, to account for the large amount of iron monosulfide present in some sediments. However, the two parameters are conceptually identical and yield the same information about iron sulfidation and availability.

4. Results

4.1. Black sea iron data

DOP data from a broad range of sediment types and depositional environments in the Black Sea are summarized in Fig. 3 and Table 2 (along with data for pyrite-S; AVS-S; and boiling, 12 N HCl-extractable Fe). Muddy turbidites in the deep euxinic margin and basin have intermediate values lying dominantly between 0.3 and 0.5, with a mean of 0.38 ± 0.04. Black, euxinic muds deposited rapidly on the basin margin just below the chemocline also show intermediate DOP values between 0.3 and 0.5, with a mean of 0.41 ± 0.05 (calculated as DOS). Unit 1 sediments collected in the deep euxinic basin have significantly higher values generally between 0.6 and 0.8, averaging 0.70 ± 0.05. Finally, sediments on the oxic/suboxic shelf, including the chemocline and paleo-chemocline (Fig. 3), show a broad range of DOP, spanning from <0.1 to values approaching 0.7. At stations characterized by relatively steady-state profiles (i.e., Stations 16, 17, 9 and 14), the lowest values tend to reflect surface intervals where diagenetic iron sulfidation is ongoing, thus explaining some of the variability in the data. The data from deeper intervals show less variability (Table 2).

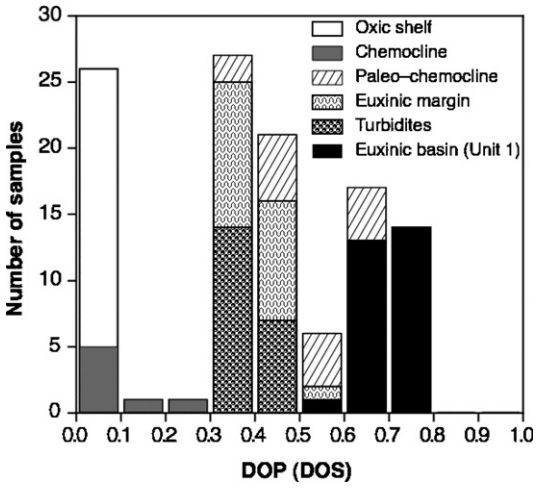

Fig. 3. Composite histogram of DOP and DOS values for sediments from the Black Sea. Distinction of sedimentary units as in Tables 1 and 2. DOS values were calculated where AVS comprises a significant proportion of the reduce sulfide pool (see Table 2) and is conceptually the same as DOP. The data show two distinct populations, representing oxic shelf sediments and deep euxinic basin sediments, and an intermediate population represents euxinic margin sediment with high siliciclastic flux, turbidites, and paleo-chemocline sediments.

Ratios of Fe_T to Al are summarized in Fig. 4 and Table 2. Ratios at stations on the oxic/suboxic shelf, the euxinic basin margin, and for turbidites in the deep basin are all in the 0.5–0.6 range. Unit 1 shows ratios spanning from roughly 0.6 to 1.2 (mean of 0.89 ± 0.16); all Unit 1 values are elevated relative to average shale/continental crust (0.5; Taylor and McLennan, 1985) and the other Black Sea stations. Data from Station 3 overlap with those from Unit 1 and with the lower, near-crustal values from the shallow oxic and euxinic settings. Ratios of Mn_T/Al are elevated above average shale (0.008) only in Unit 1 (0.021 ± 0.009) and in the bottom 12 cm of the Station 3 core (0.020 ± 0.004) (Table 2).

4.2. Orca basin and Effingham Inlet iron data

DOP data for the euxinic site in the Orca Basin are summarized in Table 2. The data scatter downcore between roughly 0.4 and 1.0, with a mean of 0.76 ± 0.19 (calculated as DOS). Pyrite-S and AVS-S concentrations are below detection ($\sim 10^{-2}$ wt%) at the transitional and oxic sites, so DOP values are nominally zero. Mean Fe_T/Al ratios at the euxinic, transitional, and oxic site are 0.63 ± 0.06, 0.93 ± 0.05, and 0.46 ± 0.02, respectively (Table 2 and Fig. 5). All the absolute weight percent concentration data for the euxinic site are tabulated on a salt-corrected dry sediment basis because of the very high salinity (~260‰) of the bottom waters. Ratios of Mn_T/Al show manganese enrichment in the euxinic site (0.016 ± 0.002) and the transitional site (0.018 ± 0.004) (Table 2). Elevated Mn_T/Al ratios are also observed in the surface 5 cm of the oxic sediments (0.020 ± 0.004), but values are close to average shale at depth (0.006 ± 0.001).

DOP (DOS) data for the oxic and euxinic sites in Effingham Inlet are summarized in Table 2, with mean values of 0.23 ± 0.05 and 0.59 ± 0.04 (DOS), respectively. Total iron and aluminum data for both sites are also summarized in Table 2. Fe_T/Al ratios average 0.61 ± 0.02 for the oxic site and 0.85 ± 0.02 for the euxinic site (Table 2 and Fig. 5). Mn_T/Al is elevated only in the euxinic site (0.014 ± 0.001) (Table 2).

5. Discussion

5.1. DOP in the Black Sea and patterns and pathways of iron enrichment

A fundamental observation for DOP, as corroborated in the Black Sea, is that high values almost universally reflect euxinic deposition, and low values typify oxic conditions (with unusual exceptions, as noted above). Intermediate DOP, however, can record *either* strongly reducing (H_2S-rich) porewaters within sediments beneath oxygen-containing bottom waters (e.g., FOAM site; Canfield et al., 1992) *or* euxinic deposition at sites of rapid siliciclastic accumulation (Black Sea Stations 5 and 15 and deep basinal turbidites at Stations 7 and the upper portion of 18A).

Table 2
Summary of Fe and S speciation and of elemental concentrations of Fe, Al, and Mn. Data for Fe_T, Al, and Mn_T are from this study, portions of the other data have been published previously (see below for data sources)

Depth (cm)	Depositional setting	S_T[a] (wt%)	AVS-S[b] (wt%)	Pyrite-S (wt%)	HCl-Fe[c] (wt%)	DOP or DOS[d]	Fe_T (wt%)	Al (wt%)	Mn_T (ppm)	Fe_T/Al	Mn_T/Al
Black Sea											
Station 3											
0–2	Oxic	0.07	b.d.l.	0.07	1.98	0.03	3.3	6.36	522	0.52	0.008
2–4	Oxic	0.15	b.d.l.	0.15	2.07	0.06	3.99	8.27	523	0.48	0.006
4–6	Paleo-chemocline	1.32	b.d.l.	1.32	1.81	0.39	4.46	7.78	489	0.57	0.006
6–8	Paleo-chemocline	3.19	b.d.l.	3.19	1.62	0.63					
8–10	Paleo-chemocline	3.23	b.d.l.	3.23	1.45	0.66	5.18	6.71	1690	0.77	0.025
10–12	Paleo-chemocline	2.41	b.d.l.	2.41	1.51	0.58	5.03	7.76	1640	0.65	0.021
12–14	Paleo-chemocline	1.19	b.d.l.	1.19	1.49	0.41					
14–16	Paleo-chemocline	2.06	b.d.l.	2.06	1.49	0.55	4.74	7.78	1220	0.61	0.016
16–18	Paleo-chemocline	1.86	b.d.l.	1.86	1.54	0.51					
18–20	Paleo-chemocline	1.52	b.d.l.	1.52	0.540	0.47	4.45	8.25	1350	0.54	0.016
Station 4											
0–2	Oxic	0.09	b.d.l.	0.09	1.89	0.04					
2–4	Oxic	0.09	b.d.l.	0.09	2.00	0.04					
4–6	Paleo-chemocline	0.81	b.d.l.	0.81	1.49	0.32					
6–8	Paleo-chemocline	1.79	b.d.l.	1.79	1.34	0.54					
8–10	Paleo-chemocline	2.28	b.d.l.	2.28	1.26	0.61					
10–12	Paleo-chemocline	2.40	b.d.l.	2.40	1.38	0.60					
12–14	Paleo-chemocline	1.50	b.d.l.	1.50	1.36	0.49					
14–16	Paleo-chemocline	1.39	b.d.l.	1.39	1.34	0.48					
16–18	Paleo-chemocline	1.15	b.d.l.	1.15	1.34	0.43					
Station 16											
0–2	Oxic	0.019	0.01	0.01	2.05	0.00	2.94	5.45	470	0.54	0.009
2–4	Oxic	0.025	0.01	0.02	2.41	0.01					
4–6	Oxic	0.044	0.01	0.04	2.10	0.01	2.72	5.45	439	0.50	0.008
6–8	Oxic	0.097		0.10	2.05	0.04					
8–10	Oxic	0.127	0.01	0.12	2.04	0.05	3.16	6.16	469	0.51	0.008
10–12	Oxic	0.103	0.01	0.09	2.04	0.04					
12–14	Oxic	0.109		0.11	1.81	0.05	2.86	5.71	438	0.50	0.008
14–16	Oxic	0.104		0.10	1.98	0.04					
16–18	Oxic	0.121		0.12	2.01	0.05	2.61	4.95	413	0.53	0.008
Station 17											
0–2	Oxic	0.016	0.01	0.01	2.96	0.00					
2–4	Oxic	0.014	0.01	0.01	2.73	0.00	4.10	7.03	549	0.58	0.008
4–6	Oxic	0.017	0.01	0.01	2.52	0.00	3.98	6.95	548	0.57	0.008
6–8	Oxic	0.034	0.01	0.03	2.43	0.01					
8–10	Oxic	0.040	0.01	0.03	2.31	0.01	3.84	6.86	571	0.56	0.008
10–12	Oxic	0.097	0.01	0.09	2.26	0.03					
12–14	Oxic	0.189	0.01	0.18	2.34	0.06	4.02	6.91	579	0.58	0.008
14–16	Oxic	0.248	0.01	0.24	2.44	0.08					
Station 16B											
0–2	Chemocline	0.124	0.09	0.03	2.45	0.07					
2–4	Chemocline	0.338	0.27	0.07	2.34	0.20					
4–6	Chemocline	0.212	0.14	0.08	2.33	0.12					
6–8	Chemocline	0.107					3.37	6.55	505	0.51	0.008
8–10	Chemocline	0.127	0.03	0.10	2.21	0.06					
10–12	Chemocline	0.360									
12–14	Chemocline	0.109	0.02	0.09	2.11	0.04					
14–16	Chemocline	0.143					3.07	6.15	489	0.50	0.008
16–18	Chemocline	0.203	0.02	0.18	1.87	0.10					
18–20	Chemocline	0.184									
20–22	Chemocline	0.146	0.02	0.13	1.86	0.06	3.06	6.17	497	0.50	0.008
Station 5											
0–2	Euxinic margin	0.587	0.39	0.20	2.48	0.32					
2–4	Euxinic margin	0.606	0.44	0.16							
4–6	Euxinic margin	0.944	0.76	0.19	2.77	0.51					
6–8	Euxinic margin	0.739	0.56	0.18			4.27	7.73	706	0.55	0.009
8–10	Euxinic margin	0.626	0.47	0.16	2.67	0.34					

Table 2 (*continued*)

Depth (cm)	Depositional setting	S_T[a] (wt%)	AVS-S[b] (wt%)	Pyrite-S (wt%)	HCl-Fe[c] (wt%)	DOP or DOS[d]	Fe_T (wt%)	Al (wt%)	Mn_T (ppm)	Fe_T/Al	Mn_T/Al
10–12	Euxinic margin	0.766	0.56	0.20			4.35	7.7	719	0.56	0.009
12–14	Euxinic margin	0.867	0.58	0.29	2.60	0.44					
14–16	Euxinic margin	0.694	0.42	0.27							
16–18	Euxinic margin	0.703	0.50	0.20	2.57	0.38					
18–20	Euxinic margin	0.581	0.39	0.19							
22–24	Euxinic margin	0.860	0.54	0.32	2.72	0.41	4.32	7.99	706	0.54	0.009
26–28	Euxinic margin	0.828	0.50	0.33							
28–30	Euxinic margin	0.734	0.50	0.23							
30–32	Euxinic margin	0.995	0.54	0.45	2.43	0.48					
34–36	Euxinic margin	0.901	0.45	0.46	2.14	0.46	4.10	7.74	622	0.53	0.008
Station 15											
0–2	Euxinic margin	0.75	0.66	0.09	2.55	0.47					
2–4	Euxinic margin	0.74	0.62	0.12	2.48	0.46					
4–6	Euxinic margin	0.80	0.57	0.22	2.52	0.44					
6–8	Euxinic margin	0.68	0.46	0.23	2.46	0.37					
8–10	Euxinic margin	0.68	0.49	0.20	2.38	0.40	3.62	6.77	545	0.53	0.008
10–12	Euxinic margin	0.63	0.41	0.22	2.57	0.33					
12–14	Euxinic margin	0.72	0.42	0.30	2.36	0.38	3.99	7.33	605	0.54	0.008
16–18	Euxinic margin	0.79	0.50	0.29	2.60	0.40	3.09	7.17	602	0.43	0.008
18–20	Euxinic margin	0.80	0.51	0.30	2.63	0.40					
22–24	Euxinic margin	0.83	0.43	0.40	2.26	0.42	3.62	6.46	528	0.56	0.008
26–28	Euxinic margin	0.86	0.40	0.47	2.48	0.38	4.17	7.44	630	0.56	0.008
34–36	Euxinic margin	0.85	0.31	0.54	2.21	0.38					
38-40	Euxinic margin	0.85	0.26	0.59	2.33	0.34	4.29	7.32	660	0.59	0.009
Station 7											
0–2	Surface fluff layer	1.40	b.d.l.	1.40	1.01	0.55					
2–4	Surface fluff layer	1.31	b.d.l.	1.31	1.39	0.45					
4–6	Turbidite	1.19	b.d.l.	1.19	1.83	0.36	4.37	8.3	785	0.53	0.009
6–8	Turbidite	1.20	b.d.l.	1.20	1.89	0.36					
8–10	Turbidite	1.12	b.d.l.	1.12	1.83	0.35	4.51	8.51	683	0.50	0.008
10–12	Buried fluff layer	1.18	b.d.l.	1.18	1.53	0.40					
12–14	Buried fluff layer	1.28	b.d.l.	1.28	1.67	0.40					
14–16	Turbidite	1.18	b.d.l.	1.18	1.84	0.36					
16–18	Turbidite	1.17	b.d.l.	1.17	1.86	0.36					
18–20	Turbidite	1.17	b.d.l.	1.17	1.81	0.36	4.44	8.44	680	0.53	0.008
20–22	Turbidite	1.13	b.d.l.	1.13	1.83	0.35					
22–24	Turbidite	1.15	b.d.l.	1.15	1.94	0.34					
24–26	Turbidite	1.12	b.d.l.	1.12	1.79	0.35					
26–28	Turbidite	1.20	b.d.l.	1.20	1.86	0.36	4.14	7.79	635	0.53	0.008
28–30	Turbidite	1.14	b.d.l.	1.14	2.01	0.33					
30–32	Turbidite	1.18	b.d.l.	1.18	2.02	0.34					
32–34	Turbidite	1.15	b.d.l.	1.15	1.98	0.34					
34–36	Turbidite	1.18	b.d.l.	1.18	1.74	0.37	4.06	7.78	634	0.52	0.008
Station 9											
2–4	Euxinic Unit 1	1.70	b.d.l.	1.70	0.62	0.71					
4–6	Euxinic Unit 1	1.42	b.d.l.	1.42	0.47	0.73					
6–8	Euxinic Unit 1	1.84	b.d.l.	1.84	0.55	0.75	2.35	2.83	487	0.85	0.017
8–10	Euxinic Unit 1	1.63	b.d.l.	1.63	0.45	0.76					
10–12	Euxinic Unit 1	1.78	b.d.l.	1.78	0.52	0.75	2.29	2.4	480	0.95	0.020
12–14	Euxinic Unit 1	1.02	b.d.l.	1.02	0.25	0.78					
14–16	Euxinic Unit 1	0.70	b.d.l.	0.70	0.20	0.75	0.83	0.69	288	1.19	0.042
16–18	Euxinic Unit 1	1.50	b.d.l.	1.50	0.38	0.78					
18–20	Euxinic Unit 1	1.24	b.d.l.	1.24	0.34	0.76	1.45	1.46	358	0.99	0.025
20–22	Euxinic Unit 1	1.62	b.d.l.	1.62	0.45	0.76					
22–24	Euxinic Unit 1	0.92	b.d.l.	0.92	0.26	0.76	1.05	1.04	298	1.04	0.029
24–26	Euxinic Unit 1	1.13	b.d.l.	1.13	0.31	0.76					
Station 14											
0–2	Euxinic Unit 1	1.21	0.06	1.21	0.78	0.58					
2–4	Euxinic Unit 1	1.53	0.04	1.53	0.83	0.62					
4–6	Euxinic Unit 1	1.44	0.03	1.44	0.68	0.65					
6–8	Euxinic Unit 1	1.69	0.04	1.69	0.73	0.67					
8–10	Euxinic Unit 1	0.99	0.03	0.99	0.40	0.68					

(*continued on next page*)

Table 2 (*continued*)

Depth (cm)	Depositional setting	S_T[a] (wt%)	AVS-S[b] (wt%)	Pyrite-S (wt%)	HCl-Fe[c] (wt%)	DOP or DOS[d]	Fe_T (wt%)	Al (wt%)	Mn_T (ppm)	Fe_T/Al	Mn_T/Al
10–12	Euxinic Unit 1	0.78	0.03	0.78	0.31	0.69					
12–14	Euxinic Unit 1	1.34	0.03	1.34	0.50	0.70					
14–16	Euxinic Unit 1	1.26	0.03	1.26	0.44	0.71					
16–18	Euxinic Unit 1	1.43	0.03	1.43	0.57	0.69					
18–20	Euxinic Unit 1	0.97	0.02	0.97	0.44	0.66	1.7	2.33	334	0.73	0.014
20–22	Euxinic Unit 1	0.76		0.76	0.39	0.63					
22–24	Euxinic Unit 1	0.97	0.03	0.97	0.42	0.67					
24–26	Euxinic Unit 1	1.24		1.24	0.64	0.63	2.03	3.08	326	0.66	0.011
Station 18A											
0–2	Surface fluff layer	1.42	b.d.l.	1.42	1.56	0.44	3.83	5.97	625	0.64	0.010
2–4	Turbidite	1.51	b.d.l.	1.51	1.75	0.43					
4–6	Turbidite	1.51	b.d.l.	1.51	1.82	0.42	4.23	6.72	680	0.63	0.010
6–8	Turbidite	1.51	b.d.l.	1.51	1.78	0.43					
8–10	Turbidite	1.50	b.d.l.	1.50	1.83	0.42	4.27	6.73	657	0.63	0.010
10–12	Turbidite	1.52	b.d.l.	1.52	1.74	0.43					
12–14	Turbidite	1.53	b.d.l.	1.53	1.70	0.44	4.2	6.56	638	0.64	0.010
14–16	Turbidite	1.53	b.d.l.	1.53	1.68	0.44	4.11	6.48	642	0.63	0.010
16–18	transition	1.52	b.d.l.	1.52	1.39	0.49					
18–20	Euxinic Unit 1	1.57	b.d.l.	1.57	0.72	0.66	2.44	3.18	453	0.77	0.014
20–22	Euxinic Unit 1	1.44	b.d.l.	1.44	0.56	0.69	2.01	2.37	391	0.85	0.016
22–24	Euxinic Unit 1	0.87	b.d.l.	0.87	0.38	0.67	1.18	1.37	278	0.86	0.020
Orca Basin											
LH996 KC8											
0–1	Oxic shelf	b.d.l.	b.d.l.	b.d.l.			2.84	5.93	1770	0.48	0.030
5–6	Oxic shelf	b.d.l.	b.d.l.	b.d.l.			3.18	6.75	1780	0.47	0.026
9–10	Oxic shelf	b.d.l.	b.d.l.	b.d.l.			3.07	6.84	369	0.45	0.005
13–14	Oxic shelf	b.d.l.	b.d.l.	b.d.l.			3.00	6.65	437	0.45	0.007
17–18	Oxic shelf	b.d.l.	b.d.l.	b.d.l.			3.05	6.68	444	0.46	0.007
23–24	Oxic shelf	b.d.l.	b.d.l.	b.d.l.			2.95	6.77	442	0.44	0.007
LH996 BC7											
0–1	Chemocline	b.d.l.	b.d.l.	b.d.l.	4.07						
1–2	Chemocline	b.d.l.	b.d.l.	b.d.l.	4.46		5.53	5.64	621	0.98	0.011
3–4	Chemocline	b.d.l.	b.d.l.	b.d.l.	5.23						
5–6	Chemocline	b.d.l.	b.d.l.	b.d.l.	4.13		5.08	5.81	1270	0.87	0.022
7–8	Chemocline	b.d.l.	b.d.l.	b.d.l.	4.09						
9–10	Chemocline	b.d.l.	b.d.l.	b.d.l.	4.13		5.00	5.72	1240	0.87	0.022
11–12	Chemocline	b.d.l.	b.d.l.	b.d.l.	4.45						
13–14	Chemocline	b.d.l.	b.d.l.	b.d.l.	4.19		5.52	5.74	1160	0.96	0.020
15–16	Chemocline	b.d.l.	b.d.l.	b.d.l.	5.34						
17–18	Chemocline	b.d.l.	b.d.l.	b.d.l.	4.32		5.67	5.72	898	0.99	0.016
19–20	Chemocline	b.d.l.	b.d.l.	b.d.l.	3.96						
20–21	Chemocline	b.d.l.	b.d.l.	b.d.l.			4.97	5.53	836	0.90	0.015
LH996 BC6[e]											
0–2	Euxinic basin	0.26	0.24	0.02	1.03	0.42					
2–4	Euxinic basin	0.60	0.57	0.03	1.46	0.69	4.93	7.96	1430	0.62	0.018
4–6	Euxinic basin	1.13	1.03	0.10	2.16	0.84					
6–8	Euxinic basin	0.43	0.34	0.09	1.33	0.48					
8–10	Euxinic basin	2.20	1.34	0.86	3.47	0.73	8.04	14.74	2333	0.55	0.016
10–12	Euxinic basin	1.30	1.23	0.07	2.59	0.83					
14–16	Euxinic basin	1.31	1.21	0.10	2.50	0.85	5.04	8.15	1244	0.62	0.015
16–18	Euxinic basin	1.24	1.17	0.07	2.41	0.85	5.19	8.63	1241	0.60	0.014
18–20	Euxinic basin	1.46	1.39	0.07	2.59	0.94	5.04	7.96	1263	0.63	0.016
20–22	Euxinic basin	0.67	0.64	0.03	1.66	0.68					
22–24	Euxinic basin	1.93	1.86	0.07	3.04	1.07	5.52	8.07	1096	0.68	0.014
24–26	Euxinic basin	1.21	1.13	0.08	2.20	0.90					
26–28	Euxinic basin	1.04	0.96	0.08	2.22	0.76	7.00	9.67	1863	0.72	0.019
28–30	Euxinic basin	0.96	0.92	0.04	1.82	0.89					
30–32	Euxinic basin	0.23	0.22	0.01	0.89	0.44					
Effingham Inlet											
EF2-GC7											
0–2	Oxic shelf			0.30	2.09		3.05	5.10	328	0.60	0.006
2–4	Oxic shelf	0.47	0.12	0.35	2.11	0.21					

Table 2 (*continued*)

Depth (cm)	Depositional setting	S_T[a] (wt%)	AVS-S[b] (wt%)	Pyrite-S (wt%)	HCl-Fe[c] (wt%)	DOP or DOS[d]	Fe_T (wt%)	Al (wt%)	Mn_T (ppm)	Fe_T/Al	Mn_T/Al
4–6	Oxic shelf	0.36	0.07	0.29	2.08	0.16					
6–8	Oxic shelf	0.46	0.04	0.42	2.16	0.17	3.40	5.79	358	0.59	0.006
8–10	Oxic shelf	0.49	0.03	0.46	2.20	0.17					
10–12	Oxic shelf	0.49	0.03	0.46	1.92	0.20					
12–14	Oxic shelf	0.49	0.03	0.46	2.20	0.17	3.58	6.09	369	0.59	0.006
14–16	Oxic shelf	0.72	b.d.l.	0.72	2.19	0.22					
16–18	Oxic shelf	0.80	b.d.l.	0.80	1.99	0.26					
18–20	Oxic shelf	1.01	b.d.l.	1.01	2.06	0.30					
20–22	Oxic shelf	0.99	b.d.l.	0.99	2.08	0.29					
22–24	Oxic shelf	0.97	b.d.l.	0.97	2.21	0.28	3.79	6.00	364	0.63	0.006
24–26	Oxic shelf	0.90	b.d.l.	0.90	2.05	0.28					
26–28	Oxic shelf	0.96	b.d.l.	0.96	2.13	0.28	3.78	6.09	370	0.62	0.006
EF1-GC3											
2–4	Euxinic basin	0.67	0.37	0.30	1.24	0.61					
4–6	Euxinic basin	0.83	0.31	0.52	1.30	0.57					
6–8	Euxinic basin	0.94	0.35	0.59	1.45	0.57	2.76	3.18	414	0.87	0.013
8–10	Euxinic basin	1.29	0.32	0.97	1.53	0.59					
10–12	Euxinic basin	1.29	0.36	0.93	1.48	0.63	3.10	3.73	514	0.83	0.014
12–14	Euxinic basin	1.49	0.27	1.22	1.27	0.66					
14–16	Euxinic basin	1.48	0.24	1.24	1.39	0.61					
16–18	Euxinic basin	1.23	0.21	1.02	1.47	0.53	3.09	3.65	546	0.85	0.015
18–20	Euxinic basin	1.62	0.26	1.36	1.44	0.63					
20–22	Euxinic basin	1.37	0.24	1.13	1.34	0.60	3.22	3.65	548	0.88	0.015
22–24	Euxinic basin		0.22		1.41						
24–26	Euxinic basin	1.26	0.22	1.04	1.39	0.56	3.10	3.73	467	0.83	0.013
26–28	Euxinic basin	1.44	0.14	1.30	1.48	0.53					
28–30	Euxinic basin	1.64	0.13	1.51	1.67	0.52					
30–32	Euxinic basin		0.10		1.73						
32–34	Euxinic basin		0.15		1.45						
34–36	Euxinic basin		0.28		1.51						

b.d.l., below detection limit.

Data sources. All Fe_T, Mn_T, and Al data are from this study. Many of the S and Fe speciation data have been published previously, although data for the shallower Black Sea stations have not been published in table format. A comprehensive list of data for the Black sea is available in Lyons (1992). Below we summarize data sources listed by station.

Black Sea St. 3 & 4: Lyons (1992), Lyons et al. (1993).
Black Sea St. 16 & 17: Lyons (1992), Lyons et al. (1993).
Black Sea St. 16B: Lyons (1992).
Black Sea St. 5: Lyons (1992), Canfield et al. (1996).
Black Sea St. 15: Lyons (1991, 1992, 1997), Hurtgen et al. (1999).
Black Sea St. 7: Lyons (1992), Lyons and Berner (1992), Canfield et al. (1996).
Black Sea St. 9 & 14: Lyons (1991, 1992, 1997), Lyons and Berner (1992), Canfield et al. (1996).
BlackSeaSt. 18A: Lyons (1991, 1992, 1997), Lyons and Berner (1992).
Orca Basin: Hurtgen et al. (1999).
Effingham Inlet: Hurtgen et al. (1999).

[a] S_T, total chromium reducible sulfur (AVS-S + pyrite-S).

[b] For cores from Black Sea Stations 3, 4, 7, 9, and 18A, concentrations were near or below the detection limit of $\sim 10^{-2}$ wt% based on sediment characteristics and representative analyses.

[c] HCl-Fe data include contributions from oxidized AVS.

[d] DOS is calculated as (1.75[AVS-S] + 0.88[Pyrite-S])/(0.88[Pyrite-S] + HCl-Fe) assuming FeS and FeS_2 stoichiometries for AVS and pyrite, respectively. DOP (for AVS-deficient sediments) is determined using the same equation but without the AVS-S term. Our approach assumes that all the AVS-Fe oxidized quantitatively to HCl-extractable phases (in the dried sample aliquot used for the HCl extraction). Although generally a valid approach, some error can result from this necessary assumption, yielding, for example, DOS values > 1.

[e] All Orca data from the euxinic site are salt corrected.

The full range of DOP data from the Black Sea, including any apparent "exceptions" to the prevailing paradigm, are readily explained in light of their depositional context. The hemipelagic Unit 1 sediments of the deep euxinic Black Sea show high values (Fig. 3) consistent with previously described Fe_{HR} enrichment (Canfield et al., 1996) and the predictions of the iron shuttle model (Wijsman et al., 2001). The data are also consistent with the paleoredox proposal of Raiswell et al. (1988) (i.e., $0.55 < DOP < 0.93$ for the most oxygen-deficient bottom waters). Similarly, DOP values for most of the sediments from the oxic to suboxic shelf are low, as predicted. Anomalously high values

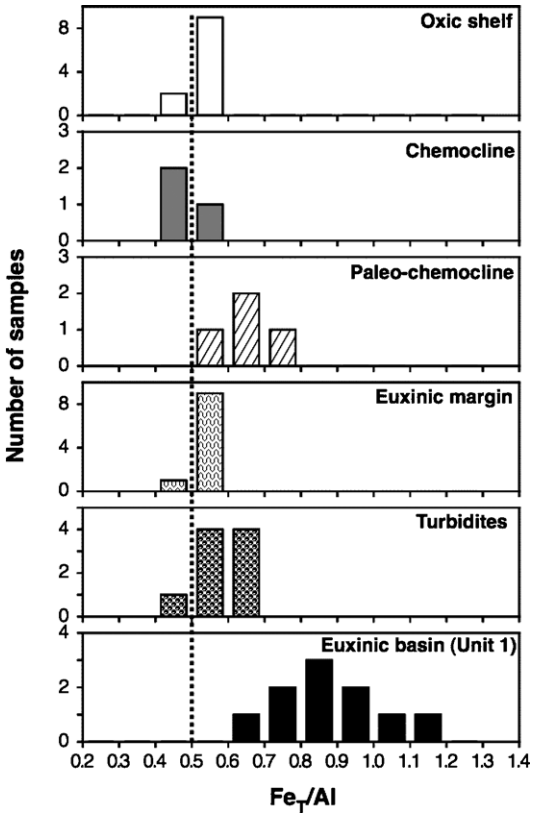

Fig. 4. Stacked histograms of Fe_T/Al ratios for Black Sea sediments. Sedimentary units are as identified in Table 2. Dashed line indicates the Fe_T/Al ratio of average shale (Taylor and McLennan, 1985). A distinct iron enrichment is evident in the euxinic sediments from Unit 1, whereas in the euxinic basin-margin and turbiditic sediments the iron augmentation is muted due to the high rates of siliciclastic sedimentation.

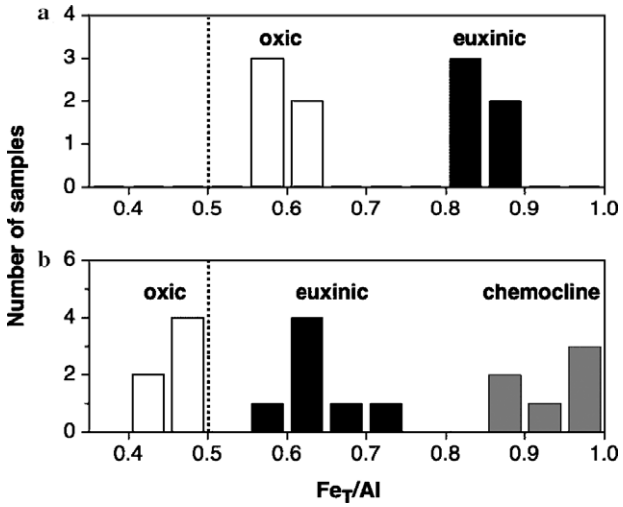

Fig. 5. Histograms of Fe_T/Al ratios for the Effingham Inlet (a) and Orca Basin (b). Similar to Fig. 4, a distinct iron enrichment is evident in the euxinic sediments relative to average shale (dashed line) and local oxic shelf sediments. Even more extreme enrichments are observed in the transitional sediments of the Orca Basin, which record deposition of iron (oxyhydr)oxide along the impingement of chemocline (and the associated iron particulate maximum) with the seafloor.

from presently oxic Stations 3 and 4 from the Bosporus region (“Paleo-chemocline” in Fig. 3, Table 2) reflect a previous episode of euxinia on the now oxic shelf as the chemocline shoaled in the recent past at least in this region (Lyons et al., 1993). In short, the iron chemistry at Stations 3 and 4 is preserving the fingerprint of past euxinia despite obliteration of sediment lamination—a common indicator of Phanerozoic oxygen deficiency—by bioturbation. Analogous enrichments are not observed in the present chemocline in the Bay of Sinop (Station 16B), suggesting that rapid vertical excursions of the chemocline and associated remobilization, as well as diffuse Fe(III) inputs, may limit present enrichment (Murray et al., 1989; Anderson et al., 1994). Also, continued shoaling of the chemocline led to euxinic conditions at Stations 3 and 4 and efficient conversion of the “new” reactive iron to pyrite, thus preserving the original Fe(III) enrichment under later reducing conditions.

The large population of euxinic data with intermediate DOP is contrary to the Raiswell et al. (1988) interpretation of restricted marine conditions for such values, which are defined as having a low but nonzero oxygen concentration. Instead, these samples record persistent euxinia at shallow and deep sites of deposition. Importantly, the laminated, AVS-rich, very rapidly accumulating muds on the basin margin have high siliciclastic fluxes that appear to swamp any iron enrichment linked to shelf export and subsequent uptake during water-column pyrite formation (Lyons, 1997; Lyons et al., 2003; Lyons and Kashgarian, 2005). As such, the total amount of iron sulfide formed and the corresponding DOP values reflect the efficient syngenetic and diagenetic sulfidation of the detritally delivered Fe_{HR} but with relatively little to no augmentation from syngenetic iron scavenging. Not coincidently, these intermediate DOP values (0.3–0.5) are very similar to those described from the highly sulfidic porewaters beneath the oxic bottom waters of the FOAM site (Canfield et al., 1992) and are also close of the ~0.4 upper limit defined for oxic sediments by Raiswell et al. (1988) and Raiswell and Canfield (1998), reflecting pyrite formation under iron-limited oxic and suboxic conditions but absent the iron enrichment that occurs only in euxinic settings. This range obviously defines the lower limit for DOP in euxinic sediments. Consistent with these observations, Canfield et al. (1996) showed Fe_{HR}/Fe_T ratios for the euxinic muds on the Black Sea margin (from our Station 5) that are virtually identical to typical oxic, continental margin sites (Raiswell and Canfield, 1998). (Note that Fe_{HR} in Canfield et al. (1996) is treated as the sum of all S-associated iron [pyrite and “FeS”], which is reasonable in this case because of the very low amounts of residual, dithionite-extractable iron.) The somewhat scattered distribution of data with a range from roughly 0.3 to 0.5 at these margin sites seems to track the reactivity of the organic carbon reservoir and, more specifically, the varying mixture of fresh, labile and reworked, refractory material. The complexities of this “secondary” control are explained in Lyons and Kashgarian (2005).

The remaining intermediate DOP values in Fig. 3 are from homogeneous, muddy turbidites collected in the deep basin. Here, redeposited muds sit in highly sulfidic porewaters beneath a euxinic water column, yet the DOP values remain intermediate (0.3–0.5) even after spending decades under these conditions. Previously, these turbiditic muds were geochemically fingerprinted to a source region on the euxinic basin margin—specifically, the rapidly accumulating black muds discussed immediately above (Lyons, 1991, 1992, 1997). It appears that the initial rapid deposition on the upper slope and subsequently during turbidite emplacement swamps any enrichment linked to syngenetic pyrite formation. Instead, iron monosulfides are transformed to pyrite with little additional sulfidation of the sedimentary iron pool (Lyons, 1997; Hurtgen et al., 1999). These turbidites provide an ideal natural experiment in which marginal sediments are injected rapidly into a deep basin setting. Despite extensive reworking, transport, and persistent additional exposure to high concentrations of H_2S, the sediments retain the overall iron properties of their euxinic margin source, including their Fe_{HR}/Fe_T ratios (Canfield et al., 1996).

5.2. Fe_T/Al ratios in the Black Sea

The shuttle model for Fe_{HR} enrichment (expressed in elevated Fe_{HR}/Fe_T ratios; Canfield et al., 1996; Raiswell and Canfield, 1998; Wijsman et al., 2001; Anderson and Raiswell, 2004) and the corresponding DOP relationships described above suggest that euxinic iron enhancement should also be seen in the Fe_T content, which is presented as Fe_T/Al ratios to minimize the complications stemming from dilution by calcium carbonate and opal. Unit 1 has a large fractionation of biogenic (dominantly coccolith) $CaCO_3$—averaging ~50 wt% (Lyons and Berner, 1992). By normalizing to Al or Ti concentrations as proxies for detrital (siliciclastic) sediment content, we can assess relative enrichments or depletions independent of dilution effects. This approach takes on added geological relevance given that mass accumulation rates (MARs; mass $area^{-1}$ $time^{-1}$), which can also correct for dilution, are generally difficult to extract from the rock record because of limited age resolution.

As predicted, Fe_T/Al ratios for Unit 1 are consistently elevated relative to the other Black Sea sediments (Fig. 4), reflecting Fe_{HR} enrichment during syngenetic pyrite formation in association with a comparatively low siliciclastic flux in the deep central basin. Conversely, the euxinic muds on the basin margin and the deep turbidites that derive from their redeposition lack Fe_T/Al evidence for iron enrichment, as was suggested from the DOP and Fe_{HR}/Fe_T data. (Fe_T/Al ratios for turbiditic mud at Station 18A are somewhat higher than those for the turbidites at Station 7.) Again, despite the possibility for some iron augmentation in the euxinic water column, any enhancement appears to be muted by the extreme rates of siliciclastic accumulation. Wilkin and Arthur (2001) showed a similar relationship, wherein Fe_T/Al ratios subtly increase with increasing water depth. The variability and low values seen in their data from the deep basin reflect the inclusion of results from Units 2 and 3 (Arthur and Dean, 1998; Huang et al., 2000) and likely turbidites.

In the absence of euxinic enrichment, sediments on the oxic/suboxic shelf have Fe_T/Al ratios (0.5–0.6) very similar to average shale (0.5; Taylor and McLennan, 1985). Finally, sediments at Station 3 show evidence for both the present oxic conditions and a past episode of euxinia linked to chemocline shoaling, thus providing confirmation that iron enrichment is also driving variations in DOP at this station.

5.3. Fe_T/Al ratios and DOP in the Orca Basin and Effingham Inlet

Extremely low DOP values at the oxic and transitional site in the Orca Basin reflect very low amounts of diagenetic H_2S production (Hurtgen et al., 1999) and the absence of sulfide in the overlying water column. Similarly, Raiswell and Canfield (1998) reported a lack of enrichment in the Fe_{HR}/Fe_T ratios for sediments that these authors classify as anaerobic/euxinic but that were deposited above the chemocline. The euxinic muds, by contrast, show high to intermediate DOP values with a nonsystematic downcore variation (Table 2). This variability must record non-steady-state properties, including inconsistent sedimentation rates. In agreement with the syngenetic Fe_{HR} enrichment suggested by the high DOP values, Fe_T/Al ratios are also elevated (~0.6 to 0.7) compared to the 0.4–0.5 values of the proximal oxic site, which are close to the average shale value.

The red muds at the transitional station, located within the chemocline, show the highest Fe_T/Al ratios measured by us in the Orca Basin (~0.85 to 1.0) despite their low DOP values. Here, the enrichment mechanism is not controlled by scavenging of dissolved iron during syngenetic pyrite formation but instead records the deposition of iron (oxyhydr)oxides along the impingement of the particulate iron maximum of the chemocline with the seafloor. This solid-phase Fe(III) maximum, fed by oxidation of $Fe(II)_{aq}$ supplied from the underlying reducing waters, is a product of extreme density stratification and iron cycling within the chemocline, as confirmed by the water-column iron profiles in Van Cappellen et al. (1998). Importantly, this enrichment is not expressed in elevated DOP values, as would be expected under euxinic conditions, thus highlighting the complementary nature of the three iron-ratio indices.

The comparatively sulfidic, oxically deposited muds in the outer basin of Effingham Inlet show DOP values ($\leqslant$0.3) consistent with partial sulfidation during diagenesis of detritally delivered Fe_{HR}. Euxinic muds in the inner basin show DOP values at the low to intermediate end of those expected under such conditions but still elevated relative to the ~0.4 lower limit for euxinic deposition. This observation, combined with Fe_T/Al ratios that are higher than those of the oxic sediments (0.8–0.9 versus ~0.6), con-

firms the likelihood of euxinic Fe_{HR} enrichment. What is surprising, however, is that this enrichment occurs despite rapid siliciclastic sedimentation at a rate roughly comparable to that along the euxinic Black Sea margin where DOP values are closer to 0.4, and Fe_T/Al and Fe_{HR}/Fe_T ratios look like those of oxic deposits. Fe_T/Al ratios in the oxic Effingham sediments are slightly elevated above average shale, suggesting an enriched detrital source that is nevertheless insufficient to explain the degree of enrichment in the euxinic sediments. These relationships suggest that parameters other than the presence or absence of sulfide in the water column and the influence of siliciclastic sedimentation rate are also imbedded in the iron paleoredox proxy, such as the mass balance relationship between the source and sink of the transported reactive iron and a high associated syngenetic pyrite flux. We note, however, that the comparatively low aluminum contents of the euxinic sediments in Effingham Inlet, rather than elevated Fe_T, appear to drive the ratio high (Table 2). Clearly, further work is needed in this unusual setting.

5.4. Testing and refining the model

5.4.1. Oxic analogs

A basic assumption of the iron shuttle model is that recycled iron exported from oxic shelves, like fine-grained sediment, will tend to concentrate in the deep basin. Accordingly, the model implies that Fe_{HR} might also be enriched in *oxic* deep basins (Raiswell and Anderson, 2005). Such a relationship will not necessarily result in high DOP values if sulfide is limiting in the pore fluids, but it could in theory challenge the uniqueness of any paleoredox predictions tied only to elevated ratios of Fe_{HR}/Fe_T and Fe_T/Al. Benthic fluxes of iron from shallow marginal sediments to the water column are well known from normal (suboxic) continental shelf sediments (Berelson et al., 2003; Elrod et al., 2004).

Perhaps the best arguments available against significant iron enrichment in deep, oxic settings come from the data compilations of Raiswell and Canfield (1998) and Poulton and Raiswell (2002). The results show average Fe_{HR}/Fe_T ratios for deep, oxic pelagic deposits from throughout the ocean, including the Mediterranean, that are comparable to those for the oxic shelf. If anything, these data reflect reactive iron *deficiencies* compared to average riverine particulates. These observations may be interpreted to indicate absence of iron mobilization in these oxic bottom water, but probably more important is the absence of a chemical trapping mechanism and an unfavorable volumetric relationship between the iron source and sink areas. The data also suggest that physical sorting phenomena are not a significant player in the enrichment of Fe_{HR}—in other words, long distance transport is not selecting in favor of a more Fe_{HR}-rich siliciclastic fraction relative to coarser Fe_{HR}-poor sediment accumulating closer to continental margins. This conclusion is supported by the observation that Fe_{HR}/Fe_T ratios for aeolian dust and oxic pelagic and continental margin settings all essential agree within error and are significantly depleted relative to many euxinic settings (Raiswell and Canfield, 1998; Poulton and Raiswell, 2002). This conclusion does not imply that physical sorting does not occur and has no relevance even on local scales (Gordon et al., 1997; Milliman et al., 1999), but rather that its effects on the Fe_{HR}/Fe_T ratio usually cannot be resolved against the background siliciclastic iron flux.

Another convincing argument against iron enrichment through physical sorting during detrital transport comes from our data in the Orca Basin. In contrast to the large distances and differing water depths that separated our stations in the Black Sea, the sites in the Orca Basin on the Gulf of Mexico continental slope are proximal to each other and essentially equidistant from the coast. Here, Fe_T/Al ratios differ markedly in sediments on either side of the oxic–euxinic interface—entirely as a function of differing water-column oxygen conditions and the efficient chemical trapping of iron below the chemocline.

Fe_T/Al ratios in the most recent sediments distributed throughout the Mediterranean Sea show locally elevated values of up to 1.05 (Table 12 in Emelyanov and Shimkus, 1986), although modern sediments in the Mediterranean are deposited under oxic conditions. There is no systematic geographic or depth trend for the Fe_T/Al ratios, making physical sorting effects unlikely. More importantly, most Fe_T/Al ratios for ancient, euxinic Mediterranean sapropels are significantly greater than the local oxic background values (e.g., Thomson et al., 1995; Warning and Brumsack, 2000), with average values for Pliocene sapropels of 1.22 (Brumsack, 2006). The elevated oxic Fe_T/Al values are therefore interpreted to reflect iron enrichment in the terrigenous source material, rather than authigenic enhancement. These findings confirm that average shale values may not always be suitable as background reference material and that local oxic sediment compositions are more appropriate, especially in enclosed basins.

Work in other ancient sediments also suggests that neither an oxic iron shuttle nor enrichment by physical sorting of particulates is a significant factor in controlling sediment iron chemistry in the ocean (e.g., Werne et al., 2002; Cruse and Lyons, 2004). In basins characterized by abrupt transitions between oxic/suboxic and euxinic deposition, as suggested independently by benthic macrofaunal ecologies, sulfur isotopes, and molybdenum concentrations, the sediments show correspondingly abrupt shifts in Fe_T/Al ratios. As for the Black Sea, the oxic sediments yield ratios of $\sim$0.5, with Fe_T and Al contents that are strongly coupled, and the euxinic intervals show highly elevated ratios and decoupled Fe_T and Al. The transitions from low to high ratios are coincident with the independently inferred changes in depositional redox—that is, the oxic sediments are not enriched in Fe_{HR}, and only through the onset of euxinia do such enrichments begin. Despite these observations,

we still do not fully understand why the source–sink–transport relationships in oxic settings preclude significant iron enrichment.

5.4.2. Iron sources, transport, and enhanced reactivity

Unlike iron, molybdenum is enriched in euxinic, suboxic, and even some oxic marine settings, and much of this enrichment occurs diagenetically through diffusion across the sediment–water interface—a process facilitated by the high concentrations of dissolved molybdenum in oxic seawater. By contrast, iron is highly insoluble in oxic seawater, and sediment enrichment requires (1) an additional source of reactive iron that is decoupled from the local detrital flux and (2) a sink for that iron via iron sulfide formation under sulfidic conditions. Thorough treatments of the source–transport–sink relationship are available in Wijsman et al. (2001), Anderson and Raiswell (2004), and Raiswell and Anderson (2005). Briefly, sediments on the oxic/suboxic Black Sea shelf are the ideal iron source. Here, elevated porewater iron concentrations (averaging 46 ± 25 μM) are sustained under low sulfide conditions; low initial organic carbon inputs and rapid iron recycling through physical and biological reworking of the surface intervals (Canfield, 1989) preclude high levels of H_2S production (Lyons, 1992; Lyons et al., 1993). The euxinic basin, by contrast, is well suited to trapping reactive iron as iron sulfide, and the absence of bioturbation and oxic recycling enhances the retention. Oxic and suboxic settings, particularly those with sulfide-deficient porewaters and high degrees of reworking and iron recycling, make better Fe_{HR} sources than sinks.

In principle, high concentrations of dissolved, shelf-derived iron in a suboxic or anoxic *but nonsulfidic* water column overlying sulfide-rich porewaters that extend to the sediment–water interface could support an iron shuttle with Fe_{HR} enrichment occurring *in the sediments*. However, we can think of no quantitatively significant examples of such environments in the modern ocean that are enriching laminated sediments in iron, including the muds within the impingement of the Black Sea chemocline. For example, organic-rich sediments of the Peru Margin that underlie upwelling regions and intercept the coastal oxygen minimum zone do not show elevated Fe_T/Al ratios or DOP values (Suits and Arthur, 2000; Böning et al., 2004), despite having anoxic bottom waters and H_2S close to the sediment–water interface.

In addition to providing an ideal iron sink, euxinic basins unlike oxic water columns could also provide an avenue for lateral transport of $Fe(II)_{aq}$ within the suboxic portions of the chemocline (Lewis and Landing, 1991). Furthermore, lateral dispersion of particulate and dissolved material can be particularly effective in these basins—as related to internal circulation patterns and the often high degrees of water-column stratification and advection along isopycnal surfaces. The basinwide continuity of millimeter-scale laminae in Unit 1 points to the tremendous efficiency in lateral transport of riverine and biogenic particulates in the Black Sea (Lyons, 1991; Lyons and Berner, 1992). Analogous processes may play an essential role in redistributing particulate iron (oxyhydr)oxides from shallow to deep settings in many euxinic basins (Raiswell et al., 2001; Raiswell and Anderson, 2005).

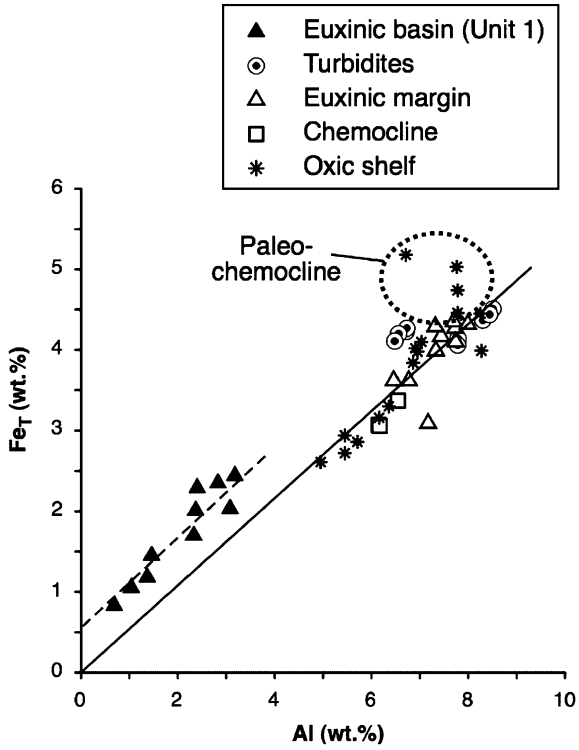

Fig. 6. Plot of Fe_T versus Al for Black Sea sediments. The relationship clearly shows the addition of externally derived, highly reactive iron under euxinic conditions. Uncorrected Fe_T concentrations, on the other hand, are lowest in Unit 1 sediments, emphasizing the need to normalize to a nonreactive detrital component in the presence of high biogenic dilution. Note that the data for the euxinic Unit 1 samples fall along a line that essentially parallels the trend of the oxic and rapidly accumulating euxinic sediments. These lines record the detrital fraction that is coupled to local aluminosilicate delivery. The positive Fe_T intercept suggests Al-decoupled iron enrichment that may be homogenous throughout the deep Black Sea.

As an alternative to the iron shuttle, Raiswell et al. (2001) hinted at the possibility that detrital iron can be significantly more pyritized under euxinic conditions. Although they cite ample contrary evidence, based largely on the protracted time scales of reactivity for Fe_{PR}, the door was left open to this possibility. Anderson and Raiswell (2004) explore this avenue further by noting that the overall reactivity of the local detrital iron pool might increase under euxinic conditions, citing poorly constrained microbial enhancement and preferential transport of fine-grained, reactive iron-enriched detrital iron to the deep basin. DOP and Fe_{HR}/Fe_T can, in theory, increase through repartitioning within the detrital iron pool via processes that enhance its reactivity but result in no net change in total iron content or Fe_T/Al ratio (Raiswell et al., 2001; Anderson and Raiswell, 2004). This process would be insensitive to siliciclastic accumulation rate. Also, elevated Fe_T/Al ratios do not preclude the possibility of increased

reactivity of the lithogenous fraction. Almost certainly this is an important although still poorly understood process that operates in combination with the iron shuttle to enrich euxinic sediments in reactive iron (Anderson and Raiswell, 2004).

Beyond iron repartitioning, any increase in Fe_T/Al ratio points uniquely to additions of *externally* derived Fe_{HR}, which seems only to occur under euxinic conditions. Importantly this iron is obviously decoupled from the local siliciclastic delivery and thus the Al content of the sediment (Fig. 6; note that the enriched samples [higher Fe_T/Al ratio] have lower overall Fe_T concentrations because of dilution by calcium carbonate). Here, the decoupled iron is expressed in the positive iron intercept. The slope of this line roughly parallels that of the oxic sediments and therefore average shale. Overall, this relationship suggests a relatively uniform enrichment across the deep euxinic basin, which is consistent with a well-mixed deep reservoir and the efficiency of lateral transport expressed in the basinwide correlation of microlaminate in Unit 1.

Recent studies of iron isotopes in continental margin sediments suggest that this novel isotopic proxy may help us refine the shelf-to-basin redox shuttle model by providing further insights into the mechanisms of euxinic iron enrichment. Some of the lowest δ^{56}Fe values to-date have been measured for porewater Fe(II) from suboxic sediments (Severmann et al., 2006), indicating that the benthic iron flux is likely to have a characteristically light iron isotope composition relative to continental weathering products. Iron isotope fractionations have been shown to occur during a wide range of equilibrium and kinetic exchange reactions (for a recent review see Anbar, 2004; Johnson et al., 2004), but theoretical predictions (Polyakov and Mineev, 2000; Schauble et al., 2001; Anbar et al., 2005) confirmed through experiments (Johnson et al., 2002) all indicate that the largest fractionations for the iron system are produced during redox transformations. These redox-dependent fractionations recorded in the benthic iron flux could be quantitatively captured under the iron-limited conditions of euxinic settings. Iron isotopes could therefore provide a unique tracer that would allow us to isotopically fingerprint the redox-driven iron shuttle.

5.4.3. Mass balance

In a follow-up to the thorough mass balance deconstruction of the Black Sea iron shuttle model of Wijsman et al. (2001), Raiswell and Anderson (2005) elegantly advanced our understanding of the iron budget by noting the strong relationship between the extent of iron addition and the ratio of the areas of shelf source (S) to basinal sink (B). Despite favorable conditions for the export of iron from the shelf and its transport and capture within the deep basin, the magnitude of enrichment within a euxinic basin is ultimately tied to the S/B ratio. Wijsman et al. (2001) and Anderson and Raiswell (2004) demonstrated that fluxes from the Black Sea shelf are adequate to explain the enrichments observed in the deep basin. Further, the data of Raiswell and Canfield (1998) and Poulton and Raiswell (2002) confirm *generally* that oxic shelves are deficient in Fe_{HR} relative to euxinic sediments, suggesting a source–sink relationship. The Fe_{HR}/Fe_T data in Canfield et al. (1996) are consistent with Fe_{HR} loss from the basin margin. Surprisingly, the shelf Fe_T/Al ratios we describe here are not depleted relative to average shale. Additional analysis from a broader array of oxic stations and characterization of the riverine flux specific to the Black Sea should speak to this disparity and the overall relevance of a comparison to average shale. Given spatial differences in watershed geology and climate, and the enrichment/depletion processes discussed here, does average shale capture average continental weathering products, average riverine particulates, or marine shales subject to iron loss and addition? It is also important to remember that sedimentation rates are significantly higher on the shelf than in the deep basin. In this regard, comparisons of *areal* extents of the shelf source and basinal sink may be less meaningful than (1) comparing time-equivalent *volumes* of the iron source to the sink or (2) thinking only in terms of the total export and import fluxes (net iron loss and gain within the basin over a given time interval). The high Fe_T/Al ratios in the euxinic sediments of Effingham Inlet remain an enigma given their very high rates of siliciclastic accumulation (Fig. 7; see discussion below). However, the small, narrow fjord has a high ratio of oxic/suboxic source to euxinic sink that strongly favors enrichment.

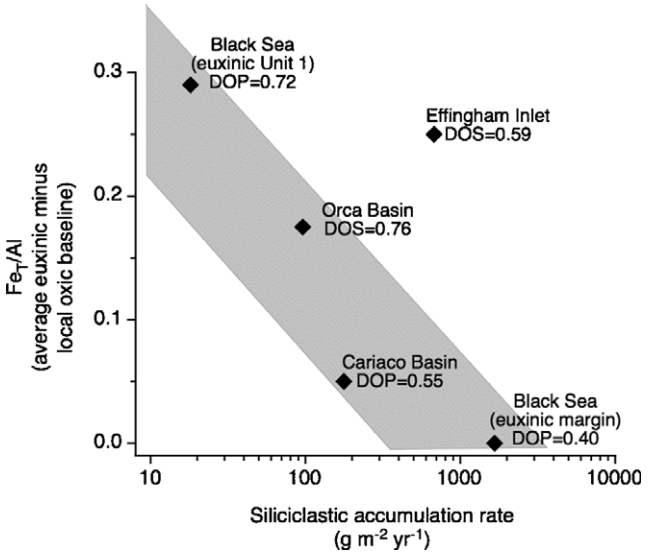

Fig. 7. Plot showing the generally inverse relationship between mean Fe_T/Al ratios and rates of siliciclastic accumulation. Fe_T/Al ratios have been corrected for small variation in the background values by subtracting the local oxic baseline value (modified from Sageman and Lyons, 2004). For the chronological framework see Calvert et al. (1991), Anderson et al. (1994), Hurtgen et al. (1999), Lyons et al. (2003), and Ingall et al. (2005). The mean Effingham Inlet Fe_T/Al ratio is significantly elevated despite high siliciclastic flux, probably reflecting its high source-to-sink ratio.

It is interesting to speculate on the implications of the S/B control on a much broader scale. Algeo (2004) and Algeo and Lyons (2006) noted that molybdenum enrichments associated with euxinia on ocean scales and within restricted basins, respectively, can be limited by molybdenum availability, and these muted enrichments can have biological implications (Anbar and Knoll, 2002). It follows that any ocean-scale euxinia would yield an S/B ratio inadequate to support large enrichments (Anderson and Raiswell, 2004); in the extreme case, the utility of the iron proxy might be compromised. As a cursory test, we looked at Fe_T/Al ratios associated with Cenomanian-Turonian Oceanic Anoxic Event 2, which shows ample independent evidence for ocean-scale euxinia. Not surprisingly, the mean C–T Fe_T/Al ratio is not greatly elevated relative to average shale (Brumsack, 2006). These ocean-scale mass balance limitations are also likely impacting the C–T molybdenum and iron data presented in Meyers et al. (2005). Mass balance constraints on the iron export model remain among the most vexing and intriguing areas of future research.

5.4.4. Relationships to rates of siliciclastic sedimentation

Canfield et al. (1996) and Raiswell and Canfield (1998) emphasized the importance of sulfide-rich, biogenic particulates as microniches that focus syngenetic pyrite formation with concomitant scavenging of dissolved iron. Consequently, siliciclastic sedimentation stifles the magnitude of enrichment by diluting the biogenous fraction (Raiswell and Canfield, 1998; Raiswell et al., 2001). Although it is less clear to us that carbonate and siliceous tests and microenvironments in general play an essential role (see discussion below), our observations in the Black Sea corroborate that rates of lithogenous accumulation under euxinic conditions are inversely related to DOP, Fe_{HR}/Fe_T, and Fe_T/Al. The likely explanation is that the rain rate of scavenged dissolved iron, which is decoupled from the local siliciclastic flux, becomes a vanishingly small part of the Fe_{HR} and Fe_T reservoirs (Fig. 1) as detrital iron fluxes increase to the levels observed on the Black Sea margin. We suspect that such effects may be common along many euxinic basin margins (Lyons and Kashgarian, 2005), and siliciclastic fluxes factor generally into all interpretations of the iron proxies (Lyons et al., 2003; Sageman and Lyons, 2004). Consistent with this effect, siliciclastic accumulation rates at euxinic sites in the Cariaco Basin, Orca Basin, and the deep and shallow Black Sea seem to correlate inversely with Fe_{HR} enrichments as expressed in Fe_T/Al ratios and, by inference, DOP and Fe_{HR}/Fe_T (Fig. 7). The euxinic site in Effingham Inlet is the only obvious exception, perhaps reflecting its high source-to-sink relationship and thus a comparatively high flux of scavenged iron.

Despite this *very general* negative correlation, we recognize that there is no single, interbasinal relationship and that other factors strongly influence iron enrichment, such as the overall mass balance between the source and the sink. Furthermore, the scavenging model is moot if the water column is not supersaturated with respect to iron sulfides. Water-column iron sulfide precipitation is well known in the Black Sea from sediment trap data (Muramoto et al., 1991), speciation studies of dissolved and particulate iron (Lewis and Landing, 1991), sulfur isotope trends (Calvert et al., 1996; Lyons, 1997), pyrite framboid size distributions (Wilkin et al., 1997; Wilkin and Arthur, 2001), and thermodynamic calculations (Landing and Lewis, 1991). The thermodynamic predictions corroborate the empirical evidence for iron sulfide precipitation—ignoring the possible effects of microenvironments—at depths of a few tens of meters below the sulfide interface. Saturation relationships are less well known for the basin margin, where the chemocline is deeper and dissolved sulfide concentrations are lower. Here, low sulfide availability may be an additional factor in limiting Fe_{HR} enrichment if syngenetic iron sulfide formation is low or absent in the overlying water. Such sulfide limitations are certainly not a factor in the deep Black Sea, including the sites of turbidite deposition, or in the deep Cariaco and Orca basins, where water-column iron sulfide formation is indicated and appears to be iron limited (Van Cappellen et al., 1998; Hurtgen et al., 1999; Lyons et al., 2003).

5.4.5. Role of particulates

A fundamental argument in the model of Canfield et al. (1996; also Raiswell and Canfield, 1998; Raiswell et al., 2001) is that euxinic enrichment of iron exported from the shelf specifically occurs through scavenging of dissolved or colloidal iron during syngenetic pyrite formation *within sulfide-rich microenvironments that are found within biogenic particles*. This assertion is grounded largely on the apparent positive covariation observed between calcium carbonate content and both Fe_{HR}/Fe_T and DOP in euxinic sediments of the Black Sea (Figs. 1b and c in Canfield et al., 1996, including data from our Stations 5, 7, 9, and 14). Canfield et al. (1996) and Raiswell and Canfield (1998) argued that high carbonate contents track the abundance of coccoliths and thus biogenous particulates with locally rapid rates of water-column sulfate reduction linked to decaying organic matter within the skeletal remains. These remains would be sites of enhanced syngenetic pyrite formation and thus enrichments in Fe_{HR} exported from the shelf. Raiswell and Canfield (1998) made the same argument for the Cariaco Basin based generally on high opal (diatom) contents.

It is clear that the covariation suggested by Canfield et al. (1996) for the Black Sea represents two distinct populations rather than a continuum of sympathetic variation, thus challenging the link between skeletal remains and iron enrichment. One group of data, which represents euxinic basin-margin muds and a deep turbidite from this study, has $CaCO_3$ contents less than 30 wt% and the low-to-intermediate DOP, Fe_{HR}/Fe_T, and Fe_T/Al values described above for these sediments. The sec-

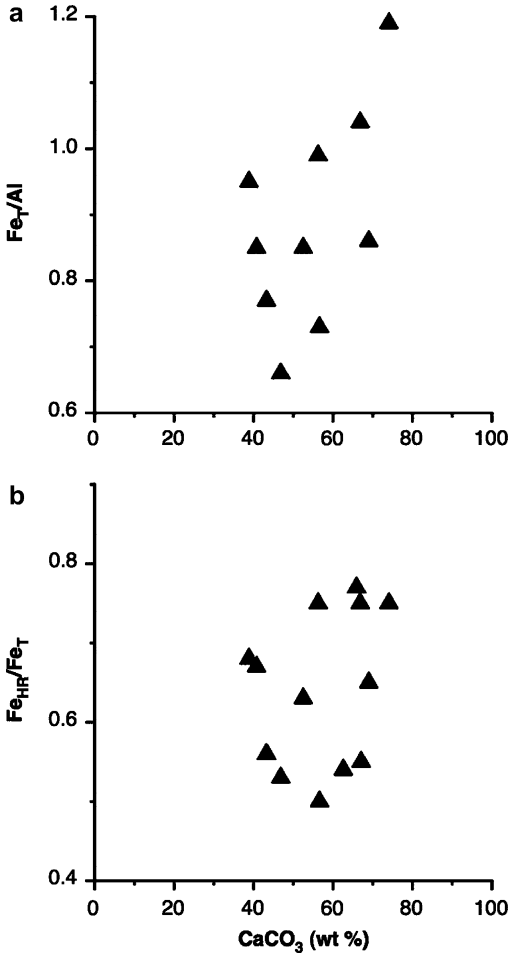

Fig. 8. Calcium carbonate contents versus (a) Fe_T/Al and (b) Fe_{HR}/Fe_T for Unit 1 sediments (Stations 9, 11, 14 and part of 18A, including data from Table 1 in Canfield et al. (1996)). Fe_{HR} is calculated as the sum of all S-associated Fe (pyrite and "FeS"). In the euxinic sediments of the Black Sea, where all highly reactive Fe-oxide has been consumed, total S-associated Fe is effectively identical to highly reactive iron (Fe_{HR}). The lack of correlation in both plots demonstrates that the reactive Fe enrichment is decoupled from the biogenic sediment input.

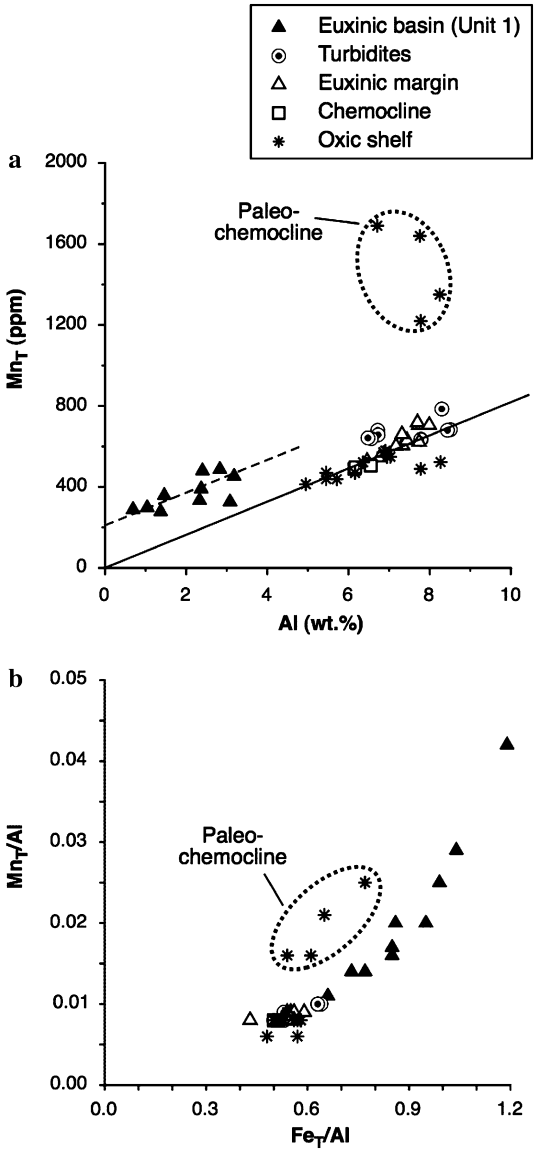

Fig. 9. (a) A plot of Mn_T versus Al for Black Sea sediments indicates that manganese is enriched in euxinic sediments, with the most extreme enrichment in the paleo-chemocline. (b) Comparison of the two elemental ratios, Mn_T/Al versus Fe_T/Al, reveals distinct co-variation with a slight curvature that implies some unknown differences in the euxinic uptake mechanisms. As for the iron data, the parallel trends and positive Mn_T intercept in Fig. 9a suggest uniform enrichment across the deep euxinic basin.

ond population is Unit 1 with $CaCO_3$ contents that generally exceed 40 wt% and with high values of DOP, Fe_{HR}/Fe_T, and Fe_T/Al. When plotted together, these data suggest a covariant relationship that is absent when the two data sets are viewed individually. More specifically, our collective Fe_T/Al and Fe_{HR}/Fe_T ratios from Unit 1 do not covary with $CaCO_3$ content (Fig. 8), and the comparatively low Fe_{HR} contents in the low $CaCO_3$ sediments could simply record rapid siliciclastic delivery relative to the rain rate of scavenged iron. In other words, the low Fe_{HR} values reflect lithogenous dilution regardless of whether the pyrite forms in direct association with local micro-sites of enhanced bacterial sulfate reduction. The consistency of small framboid diameters described for Unit 1 by Wilkin et al. (1997) and Wilkin and Arthur (2001), linked to their settling properties in the water column, is also contrary to what one might expect from pyrite formation concentrated within organic-rich aggregates with more-variable settling behavior. Furthermore, DOP values and Fe_T/Al ratios in the Cariaco Basin are not elevated within the Younger Dryas interval, despite its greater productivity expressed in higher organic carbon and opal accumulation during this period (Lyons et al., 2003). It is also unclear why localized sites of sulfide production are necessary to promote iron sulfide precipitation, given the pervasively supersaturated conditions in the water column (Lewis and Landing, 1991).

Deemphasizing the hypothesized contribution from biogenous particulates clarifies why euxinic iron enrichment is observed during time periods in the geological past when calcareous and opaline plankton where scarce or absent, including the Precambrian (Shen et al., 2003). If differences in percent biogenous material are not the primary control, other factors such as the relative spatial extents of oxic source versus euxinic sink (S/B; Raiswell and Anderson, 2005) and siliciclastic accumulation rates must regulate the magnitude of Fe_{HR} enrichment in euxinic settings.

5.4.6. Analogous manganese relationships

One of the most exciting results of this study is the support for the iron shuttle provided by complementary manganese data (Fig. 9a). The suboxic porewaters of the Black Sea oxic shelf are an ideal source of both iron and manganese. The relatively greater solubility of manganese under both oxic and sulfidic conditions increases the potential for transport to the deep basin but could also inhibit scavenging. Traditionally, euxinic sediments are noted for manganese *depletion* through $Mn(II)_{aq}$ leakage to the overlying water column (Calvert and Pedersen, 1993; Brumsack, 2006) and corresponding enrichments immediately above the impingement of the chemocline along the basin margin ("bathtub-ring" mineralization; Force and Cannon, 1988). However, concentration profiles and thermodynamic calculations suggest that Mn-sulfide supersaturation occurs in the Black Sea water column (Landing and Lewis, 1991; Lewis and Landing, 1991), and thus a mechanism for scavenging and sequestering also exists.

Our data reveal a strong positive correlation between Fe_T/Al and Mn_T/Al in the euxinic Unit 1 sediments (Fig. 9b), confirming the presence of overall manganese enrichment—likely via export from the oxic shelf. It is clear that euxinic sediments can be a net sink for manganese, at least on the scale of an individual basin. Further, our unpublished Black Sea results (Lyons, 1992) show that the ratio of manganese extracted in hydroxylamine hydrochloride/acetic acid to Mn_T is often lower in the euxinic basin than on the oxic shelf, while Mn_T/Al is enriched in the basin. The hydroxylamine hydrochloride/acetic acid combination is known to be specific to manganese bound in carbonates, oxides, and perhaps some silicates (see Lyons et al., 1993). Collectively, the results from the Black Sea suggest that manganese is efficiently lost from oxides in the deep basin while these euxinic sediments are simultaneously enriched in manganese exported from the shelf and trapped in a phase not readily extracted by the hydroxylamine hydrochloride—perhaps MnS. Further work is needed to confirm and refine this intriguing relationship. However, the positive manganese intercept and parallel Mn–Al relationships for oxic and euxinic sediments suggest comparative uniformity in the enrichment across the deep euxinic basin (Fig. 9a).

Similar manganese enrichments in the euxinic sediments of the Orca Basin and Effingham Inlet (Table 2) confirm that this proposed manganese augmentation is not unique to the Black Sea. The elevated manganese that is observed in the surface interval of the oxic sediments of the Orca Basin is interpreted as a temporary diagenetic feature marking the redoxcline (Mangini et al., 2001), which under steady-state conditions is not preserved in the deeper sediments.

5.5. Refined interpretations of ancient anoxia

The proxy strength of each of the three iron indices—DOP, Fe_{HR}/Fe_T, and Fe_T/Al—is grounded in the same principle: euxinic conditions enhance the reactive iron content of the sediments. Nevertheless, because we are looking at variations in Fe_{HR}, the Fe_{HR}/Fe_T ratio would seem to be the most sensitive measure; any Fe_{HR} augmentation will be a smaller percentage of the iron pools analyzed as part of DOP and Fe_T/Al. Given this, much of the value of Fe_T/Al lies with the abundance of data already available in the literature and the comparative ease of data generation. Many Fe_T data can be revisited from a new perspective on their paleoredox implications—without additional analysis.

A concern about the Fe_{HR}/Fe_T approach is that the fraction of Fe_{HR} extracted by dithionite may change during burial over geologic time scales. Specifically, high degrees of alteration—metamorphism, in the extreme case—result in mineralogical changes that repartition the elemental constituents. By contrast, the total amount of iron should remain constant despite any internal redistribution. Also, Fe_T/Al ratios provide a direct challenge to the possibility of solely enhanced detrital iron reactivity, rather than net iron addition, under euxinic conditions.

Although rapidly accumulating euxinic sediments can have Fe_T/Al and Fe_{HR}/Fe_T ratios like those of oxic sediments, values elevated significantly beyond those of the oxic shelf and local continental flux (and average shale, when local continental/riverine and shallow oxic marine data are not available as baselines) point unambiguously to Fe_{HR} enrichment under at least local euxinic conditions. The magnitude of this enrichment varies with the parameters outlined above, but a binary system is defined wherein any enrichment outside the scatter and uncertainty of the source material (and in the absence of secondary enhancement during burial) delineates the presence of sulfide in the water column. Secondary enrichments are known to occur, particularly in association with abrupt transitions in depositional conditions (e.g., marine versus nonmarine, normal marine versus euxinic marine). As a consequence of these environmental changes, sediments with very different properties are juxtaposed, and the resulting concentration gradients result in localized enrichments in iron sulfides and potentially Fe_{HR} (Passier et al., 1996, 1997; Lyons et al., 2003; Cruse and Lyons, 2004; Jørgensen et al., 2004). Although a source of potential paleoenvironmental ambiguity, secondary effects are typically easily distinguished

from primary euxinic deposition by their lack of lamination, highly localized mineralization, increased proportion of euhedral pyrite morphologies, and diagnostic $\delta^{34}S$ values, including highly ^{34}S-enriched samples (Middelburg, 1991; Middelburg et al., 1991; Sternbeck and Sohlenius, 1997; Wilkin and Arthur, 2001; Lyons et al., 2003; Jørgensen et al., 2004). Local, secondary iron (oxyhydr)oxide enrichments are also well known—for example, at the oxic interface in many sediment columns and along the redox transition zone in the Orca Basin (this study)—but these are easily distinguished from euxinic sediments by their low degrees of pyritization, highlighting the complementary nature of the three iron proxies.

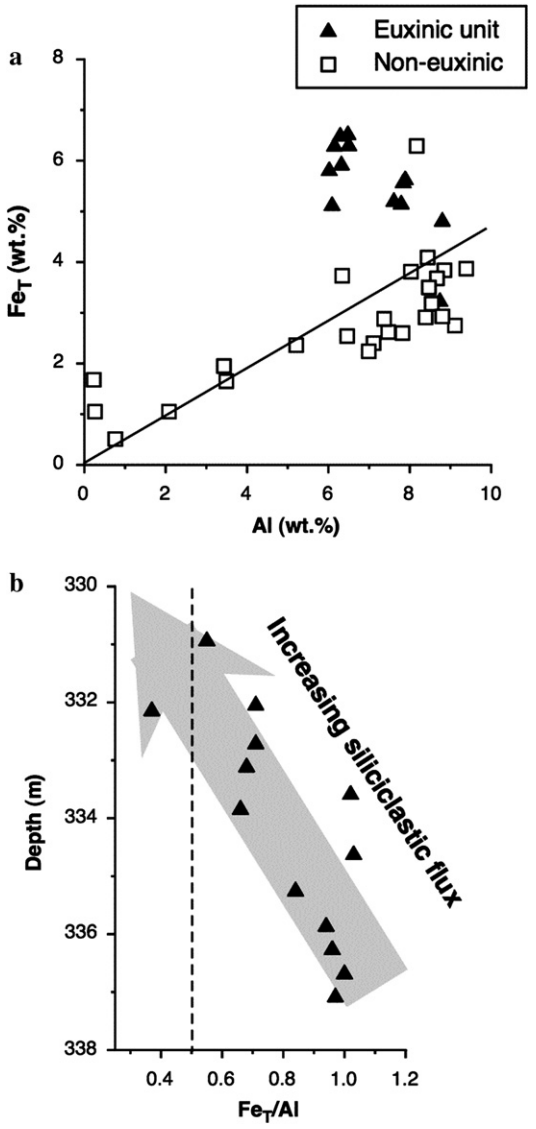

Fig. 10. (a) Plot of Fe_T versus Al for Devonian black shales from western New York (data from Werne et al., 2002). Similar to Fig. 6, the data indicate euxinic iron enrichment decoupled from the detrital flux; however, that scattered distribution suggests a less uniform pattern of enrichment. (b) Depth profile of Fe_T/Al for the Devonian euxinic unit shows a systematic up-section decrease, with ratios approaching the background average shale values (dashed line) toward the top of the unit. Independent indicators of euxinia suggest that this depth trend is due to increasing siliciclastic sedimentation over time, rather than a transition from euxinic to oxic conditions.

Poulton and Canfield (2005) expanded the extraction of Fe_{HR} to include iron in magnetite and carbonate minerals to better characterize conditions on the early Earth, specifically the Archean and portions of the Proterozoic, when dissolved iron was abundant in the O_2-poor ocean relative to limited sulfate/sulfide availability. By this refined definition, high Fe_{HR}/Fe_T ratios can reflect anoxic but noneuxinic conditions in the water column (Poulton et al., 2004b), which are also expressed in high Fe_T/Al values. However, because the boiling HCl method efficiently extracts iron in the magnetite and carbonates (Raiswell et al., 1994), theses samples would also show low degrees of pyritization.

The Fe_T/Al paleoredox proxy has already been applied with success to ancient sequences. For example, elevated ratios mark the abrupt onset of euxinia associated with Carboniferous black shales in midcontinent North America, and extreme iron enrichments suggest hydrothermal augmentation (Cruse and Lyons, 2004). Werne et al. (2002) found clear Fe_T/Al evidence for euxinic iron enrichment that was decoupled from siliciclastic delivery in the Devonian of the northern Appalachian Basin (Fig. 10). The distribution of data in Fig. 10a suggests less uniform enrichment compared to that of Unit 1 of the Black Sea (Fig. 6), which is likely indicating the relative degrees of deep-water mixing and the efficiencies of lateral transport as related to circulation and water-column stratification in the two basins. Within the Devonian sequence, a systematic, up-section stratigraphic decrease in the Fe_T/Al ratio under persistently euxinic conditions tracks independent indicators of increased aluminosilicate sedimentation (Fig. 10b). This relationship suggests more generally that if euxinia can be independently inferred, Fe_T/Al ratios can provide a means for interpreting spatial and temporal gradients in the siliciclastic flux within ancient euxinic basins. Most other geochemical tools for recognizing rapid accumulation at relatively high stratigraphic resolution, such as ^{210}Pb and ^{14}C, have limited or no value in the deep-time record. Similarly, a refined understanding of the collective controls on iron enrichment, particularly the muted effects under conditions of rapid siliciclastic sedimentation, allow us to reconcile otherwise contradictory paleoecological and geochemical indicators of paleoredox.

Because the Fe_{HR} enrichments expressed in elevated Fe_T/Al ratios are specifically a product of iron sulfide formation in the water column, and thus the presence of dissolved sulfide, we are able to distinguish between conditions of ancient anoxia/suboxia and euxinia. This distinction is not obvious by other methods, such as benthic ecological relationships that emphasize the presence or absence of preserved sedimentary lamination. However, the importance of fingerprinting euxinia increases when one

considers the negative impact hydrogen sulfide in the water column has on the seawater bioavailability of essential trace metals such as iron, molybdenum, cobalt, and zinc on basinal and oceanic scales (Anbar and Knoll, 2002; Saito et al., 2003).

6. Summary and conclusions

A reactive iron shuttle appears to operate in euxinic basins through which iron exported from the oxic shelf is sequestered in the deep basin during water-column precipitation of iron sulfides. The magnitude of enrichment is intimately linked to the ratio of the source region to the euxinic sink, and the model assumes efficient transport of particulate or dissolve iron from the shelf. Our results confirm that this mechanism results in the enrichments in highly reactive iron that are expressed in the high degrees of pyritization and the high ratios of (1) highly reactive iron to total iron and (2) total iron to aluminum observed in euxinic sediments. Euxinic Fe_T/Al and Fe_{HR}/Fe_T ratios can be two to three times great than those of normal (oxic) marine sediments and average shale. This enrichment seems not to occur under oxic conditions, nor is it imprinted strongly by physical sorting processes during transport of detrital sediment. Contrary to previous reports, enrichment is also decoupled from the relative fraction of skeletal biogenous material, such as the calcareous and opaline remains of phytoplankton. Importantly, although these enrichments appear to be a uniquely euxinic signal, they can be muted under conditions of rapid siliciclastic sedimentation. As such, a lack of enrichment records either oxic/suboxic deposition or euxinia under extreme detrital inputs. It is also possible that there is chemical or physical internal repartitioning in euxinic basin without iron gain (i.e., enhanced reactivity of the detrital fraction), thus elevating DOP and Fe_{HR}/Fe_T with potentially no impact on Fe_T/Al. The differing sensitivities of these three complementary indices of the ''iron proxy'' therefore allow us to unmix the multiple factors that impact iron distributions in euxinic basins.

The iron proxy has already shown its value for interpretations of ancient euxinia, and much of this value lies with this and other detailed calibrations in analogous modern settings, such as the Black Sea. Although mechanistic and mass balance questions remain, and it is unlikely that a single model can encapsulate the full range of controls involved, the empirical integrity of the proxy has withstood this critical evaluation and has been strengthened by the parallel trends in manganese enrichment. Because the turbidites and euxinic sediments of the Black Sea basin margin seem, at first glance, to contradict the enrichment model, a broader view of the physical properties of the sediments, including sediment accumulation rates, becomes an essential part of any paleoredox reconstruction. Further, global extents of euxinia would, from a mass balance standpoint, suppress the extent of local iron enrichment. When applied in such a context with due attention to all the controlling factors, the three iron paleoredox indices—including easily determined ratios of total iron to aluminum—provide our best inorganic signal of local euxinia.

Acknowledgments

Financial support was provided by NSF award EAR-9875961. R. Anderson generously provided unpublished data from the Black Sea, and E. Ingall coordinated and financed the sampling efforts in the Orca Basin and Effingham Inlet. The authors are grateful for their many discussions and past collaborations with D. Canfield, A. Cruse, M. Hurtgen, R. Raiswell, B. Sageman, and J. Werne. This paper was written while TL was a guest at the Max Planck Institute for Marine Microbiology. He appreciates their hospitality. The manuscript benefited from the thorough and insightful reviews of T. Anderson, R. Berner, and R. Raiswell. Most importantly, the authors thank Bob Berner for his many contributions to the field.

Associate editor: Donald Canfield

References

Addy, S.K., Behrens, E.W., 1980. Time of accumulation of hypersaline anoxic brine in Orca Basin (Gulf of Mexico). *Mar. Geol.* **37**, 241–252.

Algeo, T.J., 2004. Can marine anoxic events draw down the trace element inventory of seawater? *Geology* **32**, 1057–1060.

Algeo, T.J., Lyons, T.W., 2006. Mo-TOC covariation in modern anoxic marine environments: implications for analysis of paleoredox and -hydrographic conditions. *Paleoceanography* **21**. doi:10.1029/2004PA001112.

Aller, R.C., Mackin, J.E., Cox, R.T., 1986. Diagenesis of Fe and S in Amazon inner shelf muds: apparent dominance of Fe reduction and implications for the genesis of ironstones. *Cont. Shelf Res.* **6**, 263–289.

Aller, R.C., Hannides, A., Heilbrun, C., Panzeca, C., 2004. Coupling early diagenetic processes and sedimentary dynamics in tropical shelf environments: the Gulf of Papua deltaic complex. *Cont. Shelf Res.* **24**, 2455–2486.

Anbar, A.D., 2004. Iron isotopes: beyond biosignatures. *Earth Planet. Sci. Lett.* **217**, 223–236.

Anbar, A.D., Knoll, A.H., 2002. Proterozoic ocean chemistry and evolution: a bioinorganic bridge? *Science* **297**, 1137–1142.

Anbar, A.D., Jazecki, A.A., Spiro, T.G., 2005. Theoretical investigation of iron isotope fractionation between $Fe(H_2O)_6^{3+}$ and $Fe(H_2O)_6^{2+}$: implications for stable isotope geochemistry. *Geochim. Cosmochim. Acta* **69**, 825–837.

Anderson, R.F., Lyons, T.W., Cowie, G.L., 1994. Sedimentary record of a shoaling of the oxic/anoxic interface in the Black Sea. *Mar. Geol.* **116**, 373–384.

Anderson, T.F., Raiswell, R., 2004. Sources and mechanisms for the enrichment of highly reactive iron in euxinic Black Sea sediments. *Am. J. Sci.* **304**, 203–233.

Arnold, G.L., Anbar, A.D., Barber, T., Lyons, T.W., 2004. Molybdenum isotope evidence for widespread anoxia in mid-Proterozoic oceans. *Science* **304**, 87–90.

Arthur, M.A., Dean, S.P., 1998. Organic-matter production and preservation and evolution of anoxia in the Holocene Black Sea. *Paleoceanography* **13**, 395–411.

Arthur, M.A., Dean, W.E., Neff, E.D., Hay, B.J., King, G.M., Jones, A.D., 1994. Varve calibrated records of carbonate and organic carbon accumulation over the last 2000 years in the Black Sea. *Global Biogeochem. Cycles* **8**, 195–217.

Barbeau, K., Moffett, J.W., 2000. Laboratory and field studies of colloidal iron oxide dissolution as mediated by phagotrophy and photolysis. *Limnol. Oceanogr.* **45**, 827–835.

Berelson, W.M., McManus, J., Coale, K.H., Johnson, K.S., Burdige, D.J., Kilgore, T., Colodner, D., Chavez, F.P., Kudela, R., Boucher, J., 2003. A time series of benthic flux measurements from Monterey Bay, CA. *Cont. Shelf Res.* **23**, 457–481.

Berner, R.A., 1970. Sedimentary pyrite formation. *Am. J. Sci.* **268**, 1–23.

Berner, R.A., 1984. Sedimentary pyrite formation: an update. *Geochim. Cosmochim. Acta* **48**, 605–615.

Berner, R.A., Raiswell, R., 1983. Burial of organic carbon and pyrite sulfur in sediments over Phanerozoic times: a new theory. *Geochim. Cosmochim. Acta* **47**, 855–862.

Boesen, C., Postma, D., 1988. Pyrite formation in anoxic environments of the Baltic. *Am. J. Sci.* **288**, 575–603.

Brumsack, H.-J., 2006. The trace metal content of recent organic carbon-rich sediments: implications for Cretaceous black shale formation. *Palaeogeogr. Palaeoclimatol. Palaeoecol.* **232**, 344–361.

Böning, P., Brumsack, H.-J., Böttcher, M.E., Schnetger, B., Kriete, C., Kallmeyer, J., Borchers, S.L., 2004. Geochemistry of Peruvian near-surface sediments. *Geochim. Cosmochim. Acta* **68**, 4429–4451.

Calvert, S.E., Karlin, R.E., 1991. Relationships between sulphur, organic carbon, and iron in the modern sediments of the Black Sea. *Geochim. Cosmochim. Acta* **55**, 2483–2490.

Calvert, S.E., Karlin, R.E., Toolin, L.J., Donahue, D.J., Southon, J.R., Vogel, J.S., 1991. Low organic carbon accumulation rates in Black Sea sediments. *Nature* **350**, 692–695.

Calvert, S.E., Pedersen, T.F., 1993. Geochemistry of recent oxic and anoxic marine sediments: implications for the geological record. *Mar. Geol.* **113**, 67–88.

Calvert, S.E., Thode, H.G., Yeung, D., Karlin, R.E., 1996. A stable isotope study of pyrite formation in the Late Pleistocene and Holocene sediments of the Black Sea. *Geochim. Cosmochim. Acta* **60**, 1261–1270.

Canfield, D.E., 1989. Reactive iron in marine sediments. *Geochim. Cosmochim. Acta* **53**, 619–632.

Canfield, D.E., Raiswell, R., Bottrell, S.H., 1992. The reactivity of sedimentary iron minerals toward sulfide. *Am. J. Sci.* **292**, 659–683.

Canfield, D.E., Lyons, T.W., Raiswell, R., 1996. A model for iron deposition to euxinic Black Sea sediments. *Am. J. Sci.* **296**, 818–834.

Canfield, D.E., Raiswell, R., Westrich, J.T., Reaves, C.M., Berner, R.A., 1986. The use of chromium reduction in the analysis of reduced inorganic sulfur in sediments and shales. *Chem. Geol.* **54**, 149–155.

Chanton, J.P., Martens, C.S., 1985. The effects of heat and stannous chloride addition on the active distillation of acid volatile sulfide from pyrite-rich marine sediment samples. *Biogeochemistry* **1**, 375–385.

Cruse, A.M., Lyons, T.W., 2004. Trace metal records of regional paleoenvironmental variability in Pennsylvanian (Upper Carboniferous) black shales. *Chem. Geol.* **206**, 319–345.

Crusius, J., Anderson, R.F., 1991. Immobility of ^{210}Pb in Black Sea sediments. *Geochim. Cosmochim. Acta* **55**, 327–333.

Crusius, J., Anderson, R.F., 1992. Inconsistencies in accumulation rates of Black Sea sediments inferred from records of laminae and ^{210}Pb. *Paleoceanography* **7**, 215–227.

Dai, M.-H., Martin, J.-M., 1995. First data on trace metal level and behaviour in two major Arctic river-estuarine systems (Ob and Yenisey) and in the adjacent Kara Sea, Russia. *Earth Planet. Sci. Lett.* **131**, 127.

Elrod, V.A., Berelson, W.M., Coale, K.H., Johnson, K.S., 2004. The flux of iron from continental shelf sediments: a missing source for global budgets. *Geophys. Res. Lett.* **31**, L12307. doi:10.1029/2004GL020216.

Emelyanov, E.M., Shimkus, K.M., 1986. *Geochemistry and Sedimentology of the Mediterranean Sea*. Reidel Publishing Company, Dordrecht.

Force, E.R., Cannon, W.F., 1988. Depositional model for shallow-marine manganese deposits around black shale basins. *Econ. Geol.* **83**, 93–117.

Gordon, R.M., Coale, K.H., Johnson, K.S., 1997. Iron distributions in the Equatorial Pacific: implications for new production. *Limnol. Oceanogr.* **42**, 419–431.

Grice, K., Cao, C., Love, G.D., Böttcher, M.E., Twitchett, R.J., Grosjean, E., Summons, R.E., Turgeon, S.C., Dunning, W., Jin, Y., 2005. Photic zone euxinia during the Permian–Triassic superanoxic event. *Science* **307**, 706–709.

Hay, B.J., Arthur, M.A., Dean, W.E., Neff, E.D., Honjo, S., 1991. Sediment deposition in the late Holocene abyssal Black Sea with climatic and chronological implications. *Deep-Sea Res.* **38**, S1211–S1235.

Huang, Y., Freeman, K.H., Wilkin, R.T., Arthur, M.A., Jones, A.D., 2000. Black Sea chemocline oscillations during the Holocene: molecular and isotopic studies of marginal sediments. *Org. Geochem.* **31**, 1525–1531.

Hurtgen, M.T., Lyons, T.W., Inall, E.D., Cruse, A.M., 1999. Anomalous enrichments of iron monosulfide in euxinic marine sediments and the role of H_2S in iron sulfide transformations; examples from Effingham Inlet, Orca Basin, and the Black Sea. *Am. J. Sci.* **299**, 556–588.

Ingall, E.D., Kolowith, L., Lyons, T.W., Hurtgen, M.T., 2005. Sediment carbon, nitrogen and phosphorus cycling in an anoxic fjord, Effingham Inlet, British Columbia. *Am. J. Sci.* **305**, 240–258.

Johnson, C.M., Beard, B.L., Roden, E.E., Newman, D.K., Nealson, K.H., 2004. Isotopic constraints on biogeochemical cycling of Fe. In: Johnson, C.M., Beard, B.L., Albarède, F. (Eds.), *Geochemistry of Non-Traditional Stable Isotopes*, vol. 55. Mineralogical Society of America and Geochemical Society, pp. 359–408.

Johnson, C.M., Skulan, J.L., Beard, B.L., Sun, H., Nealson, K.H., Bratermann, P.S., 2002. Isotopic fractionation between Fe(III) and Fe(II) in aqueous solutions. *Earth Planet. Sci. Lett.* **195**, 141–153.

Jones, G.A., Gagnon, A.R., 1994. Radiocarbon chronology of Black Sea sediments. *Deep-Sea Res.* **41**, 531–557.

Jørgensen, B.B., Böttcher, M.E., Lüschen, H., Neretin, L.N., Volkov, I.I., 2004. Anaerobic methane oxidation and the deep H_2S sink generate isotopically heavy sulfides in Black Sea sediments. *Geochim. Cosmochim. Acta* **68**, 2095–2118.

Kostka, J.E., Haefele, E., Viehweger, R., Stucki, J.W., 1999. Respiration and dissolution of iron(III)-containing clay minerals by bacteria. *Environ. Sci. Technol.* **33**, 3127–3133.

Kump, L.R., Pavlov, A., Arthur, M.A., 2005. Massive release of hydrogen sulfide to the surface ocean and atmosphere during intervals of oceanic anoxia. *Geology* **33**, 397–400.

Landing, W.M., Lewis, B.L., 1991. Thermodynamic modeling of trace metal speciation in the Black Sea. In: Izdar, E., Murray, J.W. (Eds.), *Black Sea Oceanography*. Kluwer, Dordrecht, pp. 125–160.

Leventer, A., Williams, D.F., Kennett, J.P., 1983. Relationships between anoxia, glacial meltwater and microfossil preservation in the Orca Basin, Gulf of Mexico. *Mar. Geol.* **53**, 23–40.

Leventhal, J., 1983. An interpretation of carbon and sulfur relationships in Black Sea sediments as indicators of environments of deposition. *Geochim. Cosmochim. Acta* **47**, 133–137.

Lewis, B.L., Landing, W.M., 1991. The biogeochemistry of manganese and iron in the Black Sea. *Deep-Sea Res.* **38**, S773–S803.

Li, Y.-L., Vali, H., Sears, S.K., Yang, J., Deng, B., Zhang, C.L., 2004. Iron reduction and alteration of nontronite NAu-2 by a sulfate-reducing bacterium. *Geochim. Cosmochim. Acta* **68**, 3251–3260.

Lyons, T.W., 1991. Upper Holocene sediments of the Black Sea: summary of Leg 4 box-cores (1988 Black Sea Oceanographic expedition). In: Izdar, E., Murray, J.W. (Eds.), *Black Sea Oceanography*. Kluwer, Dordrecht, pp. 401–441.

Lyons, T.W., 1992. *Comparative study of Holocene Black Sea sediments from oxic and anoxic sites of deposition: geochemical and sedimentological criteria*. Ph.D. Yale University.

Lyons, T.W., 1997. Sulfur isotope trends and pathways of iron sulfide formation in the upper Holocene sediments of the anoxic Black Sea. *Geochim. Cosmochim. Acta* **61**, 3367–3382.

Lyons, T.W., Berner, R.A., 1992. Carbon–sulfur–iron systematics of the uppermost deep-water sediments of the Black Sea. *Chem. Geol.* **99**, 1–27.

Lyons, T.W., Kashgarian, M., 2005. Paradigm lost, paradigm found—The Black Sea-black shale connection as viewed from the anoxic basin margin. *Oceanography* **18**, 86–99.

Lyons, T.W., Berner, R.A., Anderson, R.F., 1993. Evidence for large pre-industrial permutations of Black Sea chemocline. *Nature* **365**, 538–540.

Lyons, T.W., Werne, J.P., Hollander, D.J., Murray, R.W., 2003. Contrasting sulfur geochemistry and Fe/Al and Mo/Al ratios across the last oxic-to-anoxic transition in the Cariaco Basin, Venezuela. *Chem. Geol.* **195**, 131–157.

Mangini, A., Jung, M., Laukenmann, S., 2001. What can we learn from peaks of uranium and manganese in deep sea sediments? *Mar. Geol.* **177**, 63–78.

Mehra, O.P., Jackson, M.L., 1960. Iron oxide removal from soils and clays by a dithionate–citrate system buffered with sodium bicarbonate. *Clays Clay Miner.* **7**, 317–327.

Meyers, S.R., Sageman, B.B., Lyons, T.W., 2005. The role of sulfate reduction in organic matter degradation and molybdenum accumulation: theoretical framework and application to a Cretaceous organic matter burial event, Cenomanian-Turonian OAE II. *Paleoceanography* **20**. doi:10.1029/2004PA001068.

Middelburg, J.J., 1991. Organic carbon, sulphur, and iron in recent semi-euxinic sediments of Kau Bay, Indonesia. *Geochim. Cosmochim. Acta* **55**, 815–828.

Middelburg, J.J., Calvert, S.E., Karlin, R.E., 1991. Organic-rich transitional facies in silled basins: response to sea-level change. *Geology* **19**, 679–682.

Milliman, J.D., Farnsworth, K.L., Albertin, C.S., 1999. Flux and fate of fluvial sediments leaving large islands in the East Indies. *J. Sea Res.* **41**, 97–107.

Moore, W.S., O'Neil, D.J., 1991. Radionuclide distributions in recent Black Sea sediments. In: Murray, J.W., Izdar, E. (Eds.), *Black Sea Oceanography*. Kluwer, Dordrecht, pp. 343–359.

Muramoto, J.N., Honjo, S., Fry, B., Hay, B.J., Howarth, R.W., Cisne, J.L., 1991. Fluxes of reduced sulfur, iron and organic carbon in the Black Sea using time-series sediment traps. *Deep-Sea Res.* **38**, S1151–S1187.

Murray, J.W., Jannasch, H.W., Honjo, S., Anderson, R.F., Reeburgh, W.S., Top, Z., Friedrich, G.E., Codispoti, L.A., Izdar, E., 1989. Unexpected changes in the oxic/anoxic interface in the Black Sea. *Nature* **338**, 411–413.

Neumann, T., Rausch, N., Leipe, T., Dellwig, O., Berner, Z., Böttcher, M.E., 2005. Intense pyrite formation under low-sulfate conditions in the Achterwasser lagoon, SW Baltic Sea. *Geochim. Cosmochim. Acta* **69**, 3619–3630.

Passier, H.F., Middelburg, J.J., van Os, B.J.H., de Lange, G.J., 1996. Diagenetic pyritisation under eastern Mediterranean sapropels caused by downward sulphide diffusion. *Geochim. Cosmochim. Acta* **60**, 751–763.

Passier, H.F., de Lange, G.J., Middelburg, J.J., Böttcher, M.E., 1997. Pyrite contents, microtextures, and sulfur isotopes in relation to formation of the youngest eastern Mediterranean sapropel. *Geology* **25**, 519–522.

Polyakov, V.B., Mineev, S.D., 2000. The use of Mössbauer spectroscopy in stable isotope geochemistry. *Geochim. Cosmochim. Acta* **64**, 849–865.

Poulton, S.W., Raiswell, R., 2002. The low-temperature geochemical cycle of iron: From continental fluxes to marine sediment deposition. *Am. J. Sci.* **302**, 774–805.

Poulton, S.W., Canfield, D.E., 2005. Development of a sequential extraction procedure for iron: implications for iron partitioning in continentally derived particulates. *Chem. Geol.* **214**, 209–221.

Poulton, S.W., Krom, M.D., Raiswell, R., 2004a. A revised scheme for the reactivity of iron (oxyhydr)oxide minerals towards dissolved sulfide. *Geochim. Cosmochim. Acta* **68**, 3703–3715.

Poulton, S.W., Fralick, P.W., Canfield, D.E., 2004b. The transition to a sulphidic ocean ~1.84 billion years ago. *Nature* **431**.

Raiswell, R., Berner, R.A., 1985. Pyrite formation in euxinic and semi-euxinic sediments. *Am. J. Sci.* **285**, 710–724.

Raiswell, R., Berner, R.A., 1986. Pyrite and organic matter in Phanerozoic normal marine shales. *Geochim. Cosmochim. Acta* **50**, 1967–1976.

Raiswell, R., Canfield, D.E., 1996. Rates of reaction between silicate iron and dissolved sulfide in Peru Margin sediments. *Geochim. Cosmochim. Acta* **60**, 2777–2787.

Raiswell, R., Canfield, D.E., 1998. Sources of iron for pyrite formation in marine sediments. *Am. J. Sci.* **298**, 219–245.

Raiswell, R., Anderson, T.F., 2005. Reactive iron enrichment in sediments deposited beneath euxinic bottom waters: constraints on supply by shelf recycling. In: McDonald, I., Boyce, A.J., Butler, I.B., Herrington, R.J., Polya, D.A. (Eds.), *Mineral Deposits and Earth Evolution*, vol. 248. Geological Society Special Publication 248, pp. 179–194.

Raiswell, R., Canfield, D.E., Berner, R.A., 1994. A comparison of iron extraction methods for the determination of degree of pyritisation and the recognition of iron-limited pyrite formation. *Chem. Geol.* **111**, 101–110.

Raiswell, R., Newton, R.J., Wignall, P.B., 2001. An indicator of water-column anoxia: resolution of biofacies variations in the Kimmeridge Clay (Upper Jurassic, U.K.). *J. Sediment. Res.* **71**, 286–294.

Raiswell, R., Buckley, F., Berner, R.A., Anderson, T.F., 1988. Degree of pyritisation of iron as a paleoenvironmental indicator of bottom-water oxygenation. *J. Sediment. Petrol.* **58**, 812–819.

Ross, D.A., Degens, E.T., 1974. Recent sediments of the Black Sea. In: Degens, E.T., Ross, D.A. (Eds.), *The Black Sea—Geology, Chemistry, and Biology*. Am. Assoc. Pet. Geol. Mem. 20, pp. 183–199.

Ross, D.A., Degens, E.T., Macllvaine, J., 1970. Black Sea: recent sedimentary history. *Science* **170**, 163–165.

Roychoudhury, A.N., Kostka, J.E., Van Cappellen, P., 2003. Pyritization: a palaeoenvironmental and redox proxy reevaluated. *Estu. Coast. Shelf Sci.* **57**, 1183–1193.

Rude, P.D., Aller, R.C., 1989. Early diagenetic alteration of lateritic particle coatings in Amazon continental shelf sediment. *J. Sediment. Res.* **59**, 704–716.

Sageman, B.B., Lyons, T.W., 2004. Geochemistry fine-grained sediments and sedimentary rocks. In: Mackenzie, F.T., Holland, H.D., Turekian, K.K. (Eds.), *Treatise on Geochemistry*, vol. 7. Elsevier, Amsterdam, pp. 115–158.

Saito, M.A., Sigman, D.M., Morel, F.M.M., 2003. The bioinorganic chemistry of the ancient ocean: the co-evolution of cyanobacterial metal requirements and biogeochemical cycles at the Archean/Proterozoic boundary? *Inorg. Chim. Acta* **356**, 308–318.

Schauble, E.A., Rossman, G.R., Taylor, H.P., 2001. Theoretical estimates of equilibrium Fe-isotope fractionations from vibrational spectroscopy. *Geochim. Cosmochim. Acta* **65**, 2487–2497.

Severmann, S., Johnson, C.M., Beard, B.L., McManus, J., 2006. The effect of early diagenesis on the Fe isotope compositions of porewaters and authigenic minerals in continental margin sediments. *Geochim. Cosmochim. Acta* **70**, 2006–2022.

Shen, Y., Knoll, A.H., Walter, M.R., 2003. Evidence for low sulphate and anoxia in a mid-Proterozoic marine basin. *Nature* **423**, 632–635.

Sheu, D.-D., 1990. The anoxic Orca Basin (Gulf of Mexico): geochemistry of brines and sediments. *Rev. Aquat. Sci.* **2**, 491–507.

Shokes, R.F., Trabant, P.K., Presley, B.J., Reid, D.R., 1977. Anoxic, hypersaline basin in the northern Gulf of Mexico. *Science* **196**, 1443–1446.

Sinninghe Damsté, J.S., Wakeham, S.G., Kohnen, M.E.L., Hayes, J.M., de Leeuw, J.W., 1993. A 6,000-year sedimentary molecular record of chemocline excursions in the Black Sea. *Nature* **362**, 827–829.

Sternbeck, J., Sohlenius, G., 1997. Authigenic sulfide and carbonate mineral formation in Holocene sediments of the Baltic Sea. *Chem. Geol.* **135**, 55–73.

Suits, N.S., Arthur, M.A., 2000. Sulfur diagenesis and partitioning in Holocene Peru shelf and upper slope sediments. *Chem. Geol.* **163**, 219–234.

Taylor, S.R., McLennan, S.M., 1985. *The Continental Crust: Its Composition and Evolution*. Blackwell, Oxford.

Thomson, J., Higgs, N.C., Wilson, T.R.S., Croudace, I.W., de Lange, G.J., Van Santvoort, P.J.M., 1995. Redistribution and geochemical

behaviour of redox-sensitive elements around S1, the most recent eastern Mediterranean sapropel. *Geochim. Cosmochim. Acta* **59**, 3487–3501.

Van Cappellen, P., Viollier, E., Roychoudhury, A.N., Clark, L., Ingall, E.D., Lowe, K., Dichristina, T., 1998. Biogeochemical cycles of manganese and iron at the oxic–anoxic transition of a stratified marine basin (Orca Basin, Gulf of Mexico). *Environ. Sci. Technol.* **32**, 2931–2939.

Warning, B., Brumsack, H.-J., 2000. Trace metals signature of eastern Mediterranean sapropels. *Palaeogeogr. Palaeoclimatol. Palaeoecol.* **158**, 293–309.

Wen, L.-S., Santschi, P., Gill, G., Paternostro, C., 1999. Estuarine trace metal distributions in Galveston Bay: importance of colloidal forms in the speciation of dissolved phase. *Mar. Chem.* **63**, 185–212.

Werne, J.P., Sageman, B.B., Lyons, T.W., Hollander, D.J., 2002. An integrated assessment of a "type euxinic" deposit: evidence for multiple controls on black shale deposition in the Middle Devonian Oatka Creek Formation. *Am. J. Sci.* **302**, 110–143.

Wijsman, J.W.M., Middleburg, J.J., Heip, C.H.R., 2001. Reactive iron in Black Sea sediments: implications for iron cycling. *Mar. Geol.* **172**, 167–180.

Wilkin, R.T., Arthur, M.A., 2001. Variations in pyrite texture, sulfur isotope compositions, and iron systematics in the Black Sea: evidence for the late Pleistocene to Holocene excursions of the O_2–H_2S redox transitions. *Geochim. Cosmochim. Acta* **65**, 1399–1416.

Wilkin, R.T., Arthur, M.A., Dean, W.E., 1997. History of water-column anoxia in the Black Sea indicated by pyrite framboid size distribution. *Earth Planet. Sci. Lett.* **148**, 517–525.